GAK and PRKCD are positive regulators of PRKN-independent mitophagy

Michael J. Munson[1,2*], Benan J. Mathai[1,2], Laura Trachsel[1,2], Matthew Yoke Wui Ng[1,2], Laura Rodriguez de la Ballina[1,2], Sebastian W. Schultz[2,3], Yahyah Aman[4], Alf H. Lystad[1,2], Sakshi Singh[1,2], Sachin Singh [2,3], Jørgen Wesche[2,3], Evandro F. Fang[4], Anne Simonsen[1,2*]

[1]Division of Biochemistry, Department of Molecular Medicine, Institute of Basic Medical Sciences, University of Oslo
[2]Centre for Cancer Cell Reprogramming, Institute of Clinical Medicine, Faculty of Medicine, University of Oslo, N-0316, Oslo, Norway.
[3]Department of Molecular Cell Biology, The Norwegian Radium Hospital Montebello, N-0379, Oslo, Norway
[4]Department of Clinical Molecular Biology, University of Oslo and Akershus University Hospital, 1478 Lørenskog, Norway

Keywords: GAK, Cyclin G Associated Kinase, PRKCD, Protein Kinase C Delta, Mitophagy, DFP, DMOG, PRKN

*Corresponding Authors:

michael.munson@astrazeneca.com
anne.simonsen@medisin.uio.no

ABSTRACT

The mechanisms involved in programmed or damage-induced removal of mitochondria by mitophagy in response to different stimuli remains elusive. Here, we have screened for regulators of PRKN-independent mitophagy using an siRNA library targeting 197 proteins containing lipid interacting domains. We identify Cyclin G-associated kinase (GAK) and Protein Kinase C Delta (PRKCD) as novel regulators of PRKN-independent mitophagy, with both being dispensable for PRKN-dependent mitophagy and starvation-induced autophagy. We demonstrate that the kinase activity of both GAK and PRKCD are required for efficient mitophagy *in vitro,* that PRKCD is present on mitochondria, and that PRKCD is required for ULK1/ATG13 recruitment to early autophagic structures. Importantly, we demonstrate *in vivo* relevance for both kinases in the regulation of basal mitophagy. Knockdown of GAK homologue (gakh-1) in *C.elegans* or PRKCD homologues in zebrafish led to significant inhibition of basal mitophagy, highlighting the evolutionary relevance of these kinases in mitophagy.

INTRODUCTION

The selective degradation of mitochondria by autophagy (mitophagy) is important for cellular homeostasis and disease prevention. Defective clearance of damaged mitochondria is linked to the development of neurodegenerative diseases such as Parkinson's disease (PD) and has also been linked to cancer[1]. Damaged mitochondria have the potential to leak dangerous reactive oxygen species causing cell damage and ultimately death, so their rapid clearance is favoured. Mitophagy involves the sequestration of mitochondria into double-membrane structures termed autophagosomes that transport and deliver material to the lysosome for degradation[2]. Elucidation of the molecular mechanisms of mitophagy has largely focused upon hereditary forms of PD and the role of the genetic risk genes *PINK1* and *Parkin* (*PRKN*) in mediating mitophagy in response to mitochondrial depolarisation [3]. Such studies have shown that selective recognition of damaged mitochondria involves PINK1-mediated phosphorylation of ubiquitin and PRKN. This further ubiquitinates outer mitochondrial membrane proteins that are recognised by specific ubiquitin-binding autophagy receptors that interact with LC3 and GABARAP proteins in the autophagy membrane to facilitate mitophagosome formation. The relative importance of this pathway *in vivo* is however not clear, as the vast majority of basal mitophagy occurring *in vivo* seems largely independent of PINK1/PRKN, as demonstrated in both mice and fly models [4,5]. Consequently, further characterisation of the mechanisms involved in PRKN-independent basal mitophagy pathways is needed to understand their role in normal physiology and disease development. One such pathway is the HIF1α/hypoxia-dependent pathway that has been particularly well characterised for the clearance of red blood cell mitochondria that occur via upregulation of the mitophagy receptor BNIP3 [6]. Several small molecules have been identified to stabilise HIF1α and replicate a hypoxia-induced mitophagy phenotype without the requirement for hypoxic conditions [7], including cobalt chloride, dimethyloxaloylglycine (DMOG) and iron chelators, with deferiprone (DFP) found to be one of the most potent [8,9].

Whilst much progress has been made in our understanding of selective autophagy and the proteins involved, little is known about the lipids and lipid-binding proteins involved in cargo recognition and autophagosome biogenesis during selective autophagy. Formation of autophagosomes relies upon a multitude of trafficking processes to manipulate and deliver lipids to the growing structure and several proteins containing lipid interaction domains have been found to play important roles in modulating autophagy [10]. Here we have carried out an imaging-based screen to examine whether human proteins containing lipid-binding domains have novel roles in HIF1α dependent mitophagy. We identify a shortlist of eleven novel and previously unknown candidates that regulate mitophagy. In particular, we show that the two kinases GAK and PRKCD are specifically required for HIF1α-dependent mitophagy without affecting PRKN-dependent mitophagy and that this regulation is also observed *in vivo* upon basal mitophagy. Therefore, these kinases represent novel targets for the study and regulation of basal mitophagy.

RESULTS

Induction and verification of mitophagy in U2OS cells

To monitor mitophagy in cultured cells, U2OS cells were stably transfected to express a tandem tag mitophagy reporter containing EGFP-mCherry fused to the mitochondrial localisation sequence (MLS) of the mitochondrial matrix protein NIPSNAP1 (hereafter termed inner MLS [IMLS] cells) in a doxycycline-inducible manner[11]. U2OS cells contain low endogenous PRKN levels that are insufficient to induce mitophagy in response to mitochondrial membrane depolarisation[12]. However, while a yellow mitochondrial network is seen under normal conditions, induction of mitophagy with the iron chelator DFP for 24 h causes movement of mitochondria to lysosomes, where the EGFP signal is quenched due to the acidic pH, leading to the appearance of red only punctate structures (Fig. 1a,b). Co-staining for the inner mitochondrial protein TIM23 verified that the EGFP-mCherry tag was localised to the mitochondrial network (Fig. 1a). To verify that the red only structures represent autolysosomes/mitolysosomes, the V-ATPase inhibitor Bafilomycin A1 (BafA1) was added for the final 2 h of DFP treatment to raise lysosomal pH and restore the EGFP signal[13]. As predicted, the number of red only structures dropped drastically (Fig. 1b). Similarly, siRNA-mediated depletion of the key autophagy inducer ULK1 before DFP addition significantly reduced the formation of red only structures (Fig. 1b). The localisation of the IMLS reporter was further validated by correlative light and electron microscopy (CLEM) following DFP treatment. Indeed, yellow network structures observed by confocal fluorescence microscopy corresponded to mitochondrial structures by EM, whereas red only structures demonstrated typical autolysosome morphologies (Fig. 1c).

DFP-induced mitophagy could be demonstrated biochemically by measuring the enzymatic activity of the mitochondrial matrix protein citrate synthase [14]. Treatment with DFP for 24 h reduced citrate synthase activity by ~40 %, which could be prevented by addition of BafA1 for the final 16 h, confirming that the reduction was due to lysosomal-mediated degradation (Fig. 1d). Finally, we were able to demonstrate by proteomic analysis that the addition of DFP for 24 h decreased the

abundance of multiple mitochondrial proteins (classified by gene ontology [GO] analysis) compared to control-treated cells (Fig. 1e). Comparison of different cellular organelles and compartments by GO annotation highlighted that mitochondrial proteins resident to the inner membrane and matrix were particularly reduced in response to DFP treatment (Fig. 1f, Supplementary Table 1). Peroxisomal protein abundance was also slightly reduced, whilst proteins belonging to the ER, lysosomes or endosomes were generally unaffected (Fig. 1f). In contrast, proteins involved in processes defined as glycolytic or mitophagy regulation showed increased abundance.

Taken together, we show that DFP treatment induces a lysosomal-dependent loss of mitochondrial proteins in U2OS cells and that mitolysosomes could be quantified by image analysis in U2OS IMLS cells.

Screening for lipid-binding protein regulators of mitophagy

To uncover the mechanisms involved in selective recognition and turnover of mitochondria in DFP treated cells we carried out an image-based siRNA screen monitoring the formation of red-only structures in response to DFP following siRNA mediated knockdown of 197 putative lipid binding proteins in U2OS IMLS cells. An initial list of proteins containing established lipid interacting protein domains (FYVE, PX, PH, GRAM, C1, C2, PROPPIN, ENTH) were identified using ExPASy Prosite (see Methods and Appendix 1). This preliminary target list was cross-examined with several U2OS proteomic datasets and restricted to proteins validated to be expressed in U2OS cells [15,16]. We included all FYVE or PX domain containing proteins due to the relevance of phosphatidylinositol 3-phosphate (PtdIns(3)P) binding proteins in autophagy initiation [17].

The primary screen was carried out using a pool containing three different siRNA oligonucleotides sequences per target. In the absence of DFP treatment, no spontaneous induction of mitophagy was observed upon gene knockdown (data not shown). In contrast, significant changes were observed with siRNA treatment in the presence of DFP, which are plotted as fold change relative to non-targeting (siNT) samples and grouped based upon lipid binding domains (Fig. 2a-e). As previously

shown, BafA1 treatment or depletion of ULK1 strongly inhibited DFP-induced formation of red (mitolysosome) structures (Fig. 1b, Fig. 2a-e red bars). Interestingly, significantly increased levels of mitophagy were seen following knockdown of HS1BP3 (Fig. 2a), a negative regulator of starvation induced autophagy that has not previously been examined in mitophagy [18]. It is interesting to note that relatively few hits from proteins containing a FYVE or PX domain were found compared to C1, C2 or GRAM domain containing proteins (Fig. 2f).

GAK and PRKCD identified as DFP mitophagy regulators by siRNA screening

To validate prospective positive and negative regulators that demonstrated significant changes in the primary screen, we selected 29 candidates for a secondary deconvolution screen where the three siRNA oligonucleotides used in the primary screen were examined individually in U2OS IMLS cells. Their effect on DFP-induced mitophagy was analysed and quantified by high-content imaging and the level of residual target mRNA was quantified by qPCR. The mitophagy phenotype of the individual siRNA oligos was then correlated to their knock-down efficiencies and compared to the mitophagy effect of the siRNA pool used in the primary screen (Supplementary Fig. 1a). As the knockdown efficiencies for some of the targets were disappointing in the secondary screen, we carried out a tertiary screen for all targets that were found to significantly affect mitophagy in the primary screen, using individual siRNA oligos at a higher concentration of siRNA (Supplementary Fig. 1b). Based on the results of the secondary and tertiary screen, we highlighted eleven targets where at least two of the three oligos had a significant effect on DFP-induced mitophagy (Fig. 3a).

To identify candidates with the highest possible relevance for mitophagy, we searched for interacting proteins for each of these eleven candidate proteins using network analysis of protein interaction data (see Methods). Interacting proteins were subjected to GO analysis and grouped based upon compartments of interest, including mitochondria, autophagy and endolysosomal compartments. The percentage of interacting proteins in each group was compared to the average percentage for all proteins screened. Of interest, AKAP13 had a high number of interactors linked to mitochondria and

autophagy. Additionally, GAK and PRKCD had higher numbers of autophagy and mitochondria linked proteins respectively than all screened proteins (Fig. 3b and Supplementary Fig. 2a,b). As several mitophagy receptor proteins involved in HIF1α-induced mitophagy are regulated by phosphorylation (including BNIP3 and BNIP3L), whilst the PINK1 kinase is dispensable for PRKN-independent mitophagy, we decided to further characterise the role of GAK and PRKCD kinases in mitophagy. In addition, GAK has been linked as a risk factor for PD [19] and PRKCD has been noted to translocate to mitochondria previously [20].

All three oligonucleotides targeting PRKCD and two of three targeting GAK caused significant inhibition of DFP-induced mitophagy in the U2OS IMLS cells (Fig. 3a, Supplementary Fig. 3). The level of citrate synthase activity was significantly decreased in DFP treated control cells, this was not the case in cells depleted of PRKCD or GAK, further indicating a reduction in mitophagy upon depletion of these kinases (Fig. 3c). Some loss of citrate synthase was still observed, likely due to incomplete target knockdown as noted by qPCR in the secondary screen (Supplementary Fig. 1a). To understand whether GAK or PRKCD localise to mitochondria upon DFP treatment, U2OS cells were treated or not with DFP and then permeabilised and fractionated by differential centrifugation to enrich for mitochondria. Successful fractionation was confirmed by enrichment of the mitochondrial proteins TIM23 and COX-IV in the mitochondrial fraction (Fig. 3d). PRKCD was strongly enriched in mitochondrial fractions under both control and DFP inducing conditions, while GAK was absent from the mitochondria fraction (Fig. 3d). Mitochondrial localisation of PRKCD was confirmed by immunofluorescence staining of endogenous PRKCD in U2OS IMLS cells, showing a striking co-localisation with the IMLS-EGFP-mCherry reporter both in the presence and absence of DFP (Fig. 3e). Upon induction of mitophagy by DFP, PRKCD was seen with red only structures, indicating it follows mitochondria to the lysosome. Indeed, western blotting confirmed the loss of PRKCD in a DFP-dependent manner that was rescued by BafA1 treatment (Fig. 3f,g). Attempts to identify endogenous GAK localisation by immunofluorescence were not successful with non-specific staining observed with all antibodies tested.

The kinase activity of GAK and PRKCD are required for functional mitophagy

As GAK and PRKCD are both serine-threonine protein kinases we next sought to determine whether their kinase activities are important for DFP-induced mitophagy. We first tested two recently published kinase inhibitors targeting GAK, IVAP1966 and IVAP1967, with a Kd of 80nM and 190nM respectively (Supplementary Fig. 4a)[21]. Concomitant dosing of IMLS cells with DFP and these GAK inhibitors demonstrated dose-dependent inhibition of mitophagy with IVAP1967, while IVAP1966 had no effect (Supplementary Fig. 4b). Fortunately, we were able to take advantage of a more potent and specific GAK inhibitor (SGC-GAK-1, termed GAKi here) with a Kd of 3.1nM and IC_{50} of 110nM, which also has a negative control probe (SGC-GAK-1N, termed GAKc here, GAK IC_{50} = >50µM) (Supplementary Fig. 4a) as well as a second control that accounts for off-target effects of GAKi (HY-19764, RIPK2 inhibitor)[22]. Using this inhibitor set, we found that DFP-induced mitophagy was significantly reduced in a dose-dependent manner with GAKi by 40% and 60% at 5 µM and 10 µM, respectively (Fig. 4a,b). By contrast, neither GAKc nor RIPK2i had an inhibitory effect (Fig. 4a,b), providing evidence that GAK kinase activity is required for functional DFP mitophagy. The effect of GAKi on mitophagy was not due to reduced cell growth during DFP treatment (Supplementary Fig. 4c).

To investigate a role of the PRKCD kinase activity in mitophagy we utilised the PKC family inhibitors (PKCi) Enzastaurin (ES) and Sotrastaurin (SS), neither of which is solely specific for PKC Delta due to isozyme similarity within the PKC family. Both compounds strongly inhibited DFP-induced mitophagy in a dose-dependent manner (Fig. 4a,b) with Enzastaurin slightly more potent than Sotrastaurin. The conventional (PRKCA, PRKCB), novel (PRKCD) and atypical (PRKCZ) PKC family members were included in the primary siRNA screen, with only siPRKCD showing significantly reduced DFP-induced mitophagy of -57% (Fig. 2c). To further investigate the potential effects of the other PKC isozymes, all PKC isoforms were depleted in the U2OS IMLS cells, which demonstrated that multiple novel PKC isoforms decreased DFP-induced mitophagy (Fig. 4c). Novel PKCs do not require calcium, but

diacylglycerol (DAG) for regulation of activity, suggesting this may be important for mitophagy. Use of pan-PKC kinase inhibitors may therefore be beneficial for exploring the role of PKC family members in DFP-induced mitophagy.

To further confirm a role for GAK and PRKCD kinase activities in mitophagy, we determined the level of citrate synthase activity following treatment with GAKi, GAKc and PKCi. As seen in Figure 4d, GAKi and PKCi both strongly blocked DFP-induced loss of citrate synthase whilst this was not seen with DMSO or GAKc control samples. Moreover, addition of GAKi or PKCi both decreased the DFP-induced loss of inner mitochondrial membrane proteins (MTCO2, COXIV, TIM23) and matrix proteins (PDH, NIPSNAP1) as examined by western blot analysis, while loss of the outer mitochondrial proteins FUNDC1 or TOM20 was generally not affected (except that GAKi blocked loss of TOM20) (Fig. 4e). This is perhaps not surprising as some outer mitochondrial proteins are known to undergo proteasomal degradation, such as MFN2, upon induction of DFP-induced mitophagy [8]. We further confirmed the loss of mitochondrial proteins by analysis of whole-cell protein abundance by mass spectrometry between DMSO and DFP treatments in the presence of GAKi and GAKc. As shown earlier, DFP treatment caused a loss of mitochondrial proteins (determined by GO Analysis), which was reduced for cells treated with GAKi, but not for GAKc, indicating that turnover of mitochondria is hindered when GAK kinase activity is blocked (Fig. 4f).

GAK and PRKCD do not regulate the HIF1α pathway

To understand how depletion or inhibition of GAK or PRKCD prevents DFP-induced mitophagy, we first examined whether treatment with GAKi or PKCi affected the HIF1α pathway. HIF1α stabilization and expression of the HIF1α responsive genes BNIP3 and BNIP3L (NIX) are important for driving mitophagy triggered by iron chelation with DFP [8,23]. As expected, BNIP3/3L mRNA and protein levels were induced upon DFP treatment with no change in HIF1α mRNA levels (Fig. 4e and Supplementary Fig. 5a,b). The expression levels of BNIP3/3L were not significantly affected by treatment with GAKi, suggesting that GAK does not regulate mitophagy through the HIF1α response. Furthermore, the

PKCi Sotrastaurin had no significant effect on BNIP3/3L expression, although Enzastaurin somewhat reduced the BNIP3L transcript level (Supplementary Fig. 5a), which may explain the relatively higher potency of Enzastaurin blocking mitophagy (Fig. 4b). We focused on Sotrastaurin for further experiments as our data indicated there was an important role for the kinase activity beyond the decrease in BNIP3L seen with Enzastaurin.

BNIP3/3L function as autophagy receptors during HIF1α induced mitophagy by recruiting ATG8 proteins through specific LC3 interacting regions (LIRs) and phosphorylation promotes their function in mitophagy [24,25]. To check whether BNIP3/3L are targets for GAK or PRKCD mediated phosphorylation, cell lysates from U2OS cells treated or not with DFP together with GAKi or PKCi were analysed using phos-tag acrylamide gels that significantly retard the migration of phosphorylated proteins [26]. Importantly, neither the protein expression of BNIP3/3L with DFP nor their migration patterns were changed in GAKi, GAKc and PKCi treated samples (Supplementary Fig. 5b), indicating that neither BNIP3 nor BNIP3L are targets for direct phosphorylation by PRKCD or GAK.

GAK and PRKCD kinase activities do not regulate PRKN-dependent mitophagy or starvation-induced autophagy

As both GAK and PRKCD regulate DFP-induced mitophagy without affecting the HIF1α pathway, we next sought to examine whether these kinases also regulated PRKN-dependent mitophagy. The U2OS IMLS-EGFP-mCherry cell line was transduced with lentivirus to constitutively overexpress PRKN (untagged), which permits strong induction of mitophagy in response to mitochondrial depolarisation such as that induced by the H^+ ionophore CCCP [27,28]. Indeed, treatment with CCCP for 16 h led to significant induction of mitophagy and near-total loss of mitochondrial network as seen by accumulation of red only structures (Fig. 5a), reduced citrate synthase activity (Fig. 5b) as well as the loss of the mitochondrial matrix protein PDH, along with PRKCD that also localises on mitochondria (Fig. 5c,d). Importantly, we could block PRKN-dependent CCCP-induced mitophagy by co-treatment

with the ULK1/2 inhibitor MRT68921 or the lysosomal inhibitor BafA1 (Fig. 5a-d) [13,29]. Co-treatment with GAKi, GAKc or PKCi had no effect (Fig. 5a-d), suggesting that GAK and PRKCD kinase activities are dispensable for PRKN-mediated mitophagy under these conditions. We next considered whether GAKi or PKCi could impair starvation-induced autophagy. Cells were incubated in nutrient starvation media (EBSS) for 2 h and the autophagic flux examined by immunostaining for endogenous LC3B in the absence or presence of BafA1, as analysed by fluorescence microscopy (Fig. 5e,f) or immunoblotting (Fig. 5g). Whilst incubation in EBSS increased LC3 flux relative to the control, addition of GAKi or GAKc to EBSS treated cells did not significantly inhibit the autophagic flux. PKCi caused elevated LC3-II levels in the absence of BafA1.

Taken together, we show that while GAK and PRKCD kinase activities are required for efficient DFP-induced mitophagy, but are dispensable for PRKN-dependent mitophagy and starvation-induced autophagy.

PRKCD inhibitors reduce ULK1 initiation complex assembly

To further elucidate how GAK or PRKCD kinase inhibition may block DFP-induced mitophagy, we examined the recruitment of core autophagy machinery components to mitochondria. U2OS IMLS cells treated with DMSO or DFP were immunostained for endogenous ATG13, LC3B, ULK1 or WIPI2 and examined by confocal microscopy. In many cases, the early autophagosome structures induced by DFP treatment were localised at or close to mitochondria, likely representing mitophagosome start sites (Fig. 6a-d). Using high-content imaging we found that formation of WIPI2, ATG13 or ULK1 puncta were all strongly induced (~5-fold) in response to 24h DFP treatment (Fig. 6e,f, Supplementary Fig. 6a-d). Treatment with GAKi or GAKc did not affect the number of WIPI2, ATG13 or ULK1 puncta observed following 24 h of DFP treatment (Fig. 6e,f, Supplementary Fig. 6a-d). Moreover, neither GAKi nor GAKc affected phosphorylation of ULK1 at S555 (AMPK site) or S757 (mTOR site) (Supplementary Fig. 6e), suggesting that GAK regulates DFP-induced mitophagy through

a different mechanism. Interestingly, control cells treated with GAKi only (no DFP) displayed an increased number of WIPI2 puncta (Supplementary Fig. 6a,d), but the reason for this is not apparent.

Most importantly, co-treatment of cells with DFP and PKCi caused a dose-responsive decrease in the number and size of ULK1 and ATG13 puncta (and to a lesser extent WIPI2 though this was not significant) (Fig. 6e,f and Supplementary Fig. 7d). However, neither the phosphorylation of ATG13 at S318 (a known ULK1 site) [30] or the phosphorylation of AMPK at T172 (an activation site) [31] that occur in response to DFP treatment were impaired or altered by co-treatment with GAKi, GAKc or PKCi (Fig. 4e). We thus conclude that the kinase activity of PRKCD is required for successful assembly and formation of the ULK1 complex during DFP-induced mitophagy, but that it does not affect ULK1 activity directly. As PRKCD is localised to mitochondria, a failure to generate an initiation structure upon its depletion or inactivation likely explains the reduced level of mitophagy observed.

GAK inhibition alters mitochondrial morphology

As GAK inhibition did not affect HIF1α signalling, ULK1 activity or ATG13/ULK1 recruitment, we next examined mitochondrial morphology. IMLS cells co-treated with DFP and siGAK (Supplementary Fig. 3) or GAKi (Fig. 4a) demonstrated abnormal mitochondrial network structures compared to control cells. Using live-cell microscopy, we observed a collapsed mitochondrial network with clumped mitochondrial regions and reduced red structures in IMLS cells co-treated with DFP and GAKi that were not seen with GAKc (Supplementary Movie 1). Confocal microscopy confirmed this and by contrast, cells co-treated with DFP and PKCi retained an elongated network (Fig. 7a). Cells treated with a combination of Oligomycin and Antimycin A (O+A) or CCCP, known to depolarize mitochondria, caused fragmented network phenotypes (Fig. 7a). In the latter case, little mitophagy is seen in response to mitochondrial depolarisation as this was carried out in IMLS cells without PRKN overexpression. To quantify mitochondria morphology, images of U2OS cells depleted of the fission enzyme DRP1 or the fusion enzyme OPA1 (causing tubulated or fragmented mitochondrial phenotypes respectively, Supplementary Fig. 7), were applied to train a cell classifier in CellProfiler

Analyst. Applying this, we confirmed that GAKi treated cells exhibit a hyper fused mitochondria phenotype while no morphological differences were detected in GAKc or PKCi treated samples (Fig. 7b). The observed GAKi phenotype was not caused by a general defect in the fission/fusion rate of the mitochondrial network, as mitochondrial fragmentation could still be induced by co-treatment of GAKi with DFP and CCCP (Fig. 7c). Importantly, GAKi still prevented the formation of red only structures under such conditions, indicating that GAK is important for proper uptake of fragmented mitochondria into autophagosomes.

We next examined GAKi treated U2OS IMLS cells by CLEM. Interestingly, this showed condensed parallel layers of mitochondria that were not fused, but rather stacked closely with one another (Fig. 7d). Additionally, large autolysosome structures were observed, which may indicate lysosomal defects following GAKi treatment (Fig. 7d). Indeed, an increase in the number of lysosomal structures was detected in cells stained for the late endosome/lysosome marker LAMP1 following co-treatment with DFP and GAKi (Fig. 7e,f). As GAKi did not inhibit PRKN-dependent mitophagy (Fig. 5a-d) or starvation-induced autophagy (Fig. 5e-g) we reasoned that the large autolysosomes seen in GAKi treated cells retain their acidity and degradative capacity. In line with this, lysotracker positive structures were detected in cells treated with GAKi or GAKc in the presence or absence of DFP (Fig. 7g). Thus, we believe that the mitophagy defect induced by GAKi is due to inefficient cargo loading or delivery to lysosomes rather than a lysosomal defect.

Mass Spectrometry with GAKi

To try to identify relevant substrates for GAK kinase-dependent regulation of DFP-induced mitophagy, we carried out phospho-proteomic analysis of cells treated with DFP in combination with GAKi or GAKc. GAK is currently defined as an understudied kinase [32] and GAKi was developed by the SGC consortium to reveal novel understandings of GAK cellular function [22]. Analysis of both the protein abundance and phospho-sites of interest (Fig. 8a) demonstrated that DFP treatment increased the abundance of several proteins in a GAKi independent manner, including HIF1α, BNIP3L,

Hexokinase I/II, LAMP1/2 and LC3B. In contrast, SQSTM1 abundance decreased in response to DFP even with GAKi, further showing that lysosomes are functional in this state. Interestingly, phosphorylation of RAB7A at S72 was observed in response to DFP treatment. The same RAB7A modification was recently reported to facilitate a key step in PRKN-dependent mitophagy, suggesting that similarities exist during DFP mitophagy [33]. RAB14 was also phosphorylated (at S180) in response to DFP, a change that may be interesting to examine further.

GAKi-dependent changes in phosphorylation were also seen, we observed a very specific loss of clathrin light chain A (CLTA) phosphorylation at S105. This site lies at the interface between the clathrin heavy and light chains, supporting a previously described role of GAK in clathrin-cage uncoating. Increased levels of PGK1 S203, PGM1 S117 and PGM2 S165 (established phosphorylation sites to induce glycolysis) were detected upon GAKi treatment without DFP, suggesting that glycolysis may be higher at the basal state. We also see higher DRP1 S616 levels with GAKi and DFP, a modification normally associated with increased fission activity that can be mediated by CDK1 [34]. Moreover, SQSTM1 phosphorylation at S272 is increased with GAKi, also previously noted to be mediated by CDK1 [35], suggesting that GAKi treatment increases CDK1 activity and may indicate increased cell numbers in mitosis [36].

GAK and PRKCD modulate mitophagy *in vivo*

Knockout of GAK orthologues have been shown to cause embryonic lethality in mice, *C.elegans* (*dnj-25*) and *D.melanogaster* (*dAux*), which is postulated to occur due to defective clathrin-dependent endocytosis, as uncoating of clathrin-coated vesicles is mediated by the J-domain of GAK [37–39]. Indeed, expression of the J-domain alone is able to rescue survival in both mice and drosophila GAK knockout models [39,40]. *C.elegans* contains two orthologues of GAK, comprising the kinase domain (gakh-1, F46G11.3, 40% overall homology) or the J-domain (dnj-25, W07A8.3, 49% overall homology) (Fig. 8b), where targeting of the latter by RNAi causes lethality during larval development [38]. As our data indicate a requirement of GAK kinase activity for efficient mitophagy in

mammalian cells, we examined the effect of targeting gakh-1 upon basal mitophagy in a *C.elegans* reporter line expressing mtRosella GFP-DsRed in body wall muscle cells, following the concept of the IMLS reporter cell lines. *C.elegans* fed gakh-1 RNAi demonstrated a significant decrease in the ratio of GFP to DsRed and more mitophagy events (DSRed only structures, Fig. 8c) compared to the RNAi control, confirming that GAK kinase activity is important for basal mitophagy *in vivo*.

We next sought to examine the role of PRKCD in mitophagy *in vivo* and targeted Prkcd in our recently established transgenic mitophagy reporter zebrafish line, expressing zebrafish Cox8 fused to EGFP-mCherry (Abudu et al., 2019). Zebrafish contain paralogues (prkcda and prkcdb) that are ~80% similar to one another and ~76% homologous to human PRKCD, with all major domains being highly conserved (Fig. 9a). We examined the spatio-temporal expression pattern of *prkcda* and *prkcdb* during zebrafish development up until 5 days post-fertilisation (dpf). Whilst a high level of maternal *prkcd*a mRNA was observed at 2 hours post fertilisation (hpf), possibly indicating a role in early embryonic signalling events, both genes were expressed at similar levels throughout development (Fig. 9b). The spatial distribution of *prkcda* and *prkcdb* were analysed by whole-mount *in situ* hybridisation (WM-ISH) at 5 dpf compared to a sense probe negative control and showed strong staining in the corpus cerebelli region of the hindbrain for both genes (Fig. 9c, Supplementary Fig. 8a), this is in agreement with ISH data deposited in the ZFIN database (http://zfin.org). *prkcda* expression was also detected in the eyes and the olfactory bulbs (Fig. 9c) whereas *prkcdb* was found in patches of the retina, optical tectum and the spinal cord (Fig. 9c). We also analysed the spatio-temporal pattern of *gak* expression across zebrafish development and observed that even though it is expressed consistently throughout development (Supplementary Fig. 8b), its spatial expression pattern varies across development with staining of the caudal hindbrain and retina at 2 dpf, the optical tectum, neurocranium, retina and kidney at 3dpf, the kidney and neurocranium at 4dpf and the liver, olfactory bulb, optical tectum and retina at 5dpf of the wild type zebrafish larvae, with no staining of the control probe (Supplementary Fig. 8c).

To investigate a possible role for Prkcd in the mitophagy reporter line, we employed CRISPR/Cas9-mediated genome editing in zebrafish embryos using guide sequences targeting *prkcda* and *prkcdb* individually or together (Fig. 9d and Supplementary Fig. 8d), with the latter referred to as *prkcd_ab* double knock-out (DKO). We verified loss of Prkcd protein levels in DKO embryos by western blot (Fig. 9d) and therefore used these embryos for *in vivo* mitophagy analysis.

To induce mitophagy, zebrafish larvae at 2 dpf were incubated with varying concentrations of DFP and DMOG for 24 hours. DFP failed to induce mitophagy at all concentrations, however, DMOG induced mitophagy as shown by reduced levels of Tim23 (Supplementary Fig. 8e,f), in line with a recent report [41]. We used 100 µM DMOG for further experiments, as significant lethality and morphological defects were present at higher (250 µM) concentrations (Supplementary Fig. 8g). As *prkcd_a/b* express highly in the hindbrain (Fig. 9c), we examined mitophagy in this region of DKO larvae compared to control larvae, both at basal (DMSO) and DMOG-treated conditions. Sections of fixed larva were imaged by confocal microscopy and the number of red puncta in the hindbrain region quantified. The number of red only puncta was significantly reduced in the hindbrain of DKO larvae with both basal and DMOG-induced conditions (Fig. 9e,f), showing an important role of Prkcd_a/b in regulating mitophagy. Interestingly, we noticed the lack of a properly formed eye-lens in one of the two eyes of the *prkcd_ab* DKO, with considerably reduced mitophagy levels when compared to the control (Supplementary Fig. 8h). We also observed an inconsistent and varied movement pattern of the DKO larvae, and therefore quantified their locomotor activity. Tracking and quantification of locomotion was performed in alternating light and dark conditions with a reduced swimming trend in the dark phase for both Prkcd single KO and DKO larvae compared the WT control (Fig. 9g). It is likely that this may be related to the observed lens defect or a hindbrain clustered motor-neuron dependent phenotype.

In conclusion, we show that the activity of both GAK and PRKCD is important for regulation of basal mitophagy *in vivo*, highlighting the evolutionary relevance of these kinases in mitophagy.

DISCUSSION

In this manuscript, we have tested a panel of putative lipid-binding proteins for their ability to regulate DFP-induced mitophagy. We have identified eleven candidate proteins that demonstrate significant modulation of DFP-induced mitophagy and explored two of these, GAK and PRKCD, in further detail. In both cases, we show that functional kinase activity is required for their positive regulation of DFP-induced mitophagy and we have identified putative mechanisms for how each function in mitophagy regulation. Importantly, neither GAK nor PRKCD are required for PRKN-dependent mitophagy or starvation-induced autophagy, offering novel targets for the specific modulation of PRKN-independent mitophagy. Critically, we find that both of these targets identified *in vitro* are also relevant targets *in vivo* for the regulation of basal mitophagy in *C.elegans* and *D.rario,* demonstrating their conserved function in mitophagy.

The linkage of GAK to mitophagy is of particular relevance to neurodegenerative disease as SNPs in GAK have previously been identified as a risk factor for familial PD [19] and expression changes in GAK are observed in the substantia nigra of PD patients [42]. Knockout of the drosophila homologue of GAK (Auxilin) also demonstrates Parkinsonian like mobility defects and loss of dopaminergic neurons [43]. Further work has shown that the commonly mutated PD gene, LRRK2, can phosphorylate Auxilin[44]. Studies of GAK have to date, however, been hindered by the limited availability of chemical tools alongside the inherent difficulty of modulating embryonic lethal genes to dissect their function. *C.elegans* presents a unique opportunity for the *in vivo* study of GAK kinase function due to the presence of two orthologues of human GAK, with the homologous kinase domain within a separate protein (gakh-1) than that of the developmentally essential J-domain (dnj-25) [38]. By knockdown of gakh-1, we were able to see >50% reduction in basal mitophagy in muscle-cell wall highlighting the importance of GAK for mitophagy. Further investigation is required to mechanistically ascertain how this functional effect is mediated, as Hif1α induction and subsequent recruitment of ULK1/ATG13 to mitophagosomes in response to DFP stimulation appears normal in cells with GAK kinase activity

inhibited. However, we observed a significant disruption of mitochondrial network morphology which may modulate the ability of mitochondria to be loaded correctly into mitophagosomes. Artificially inducing mitochondrial fragmentation with CCCP, however, was not sufficient to rescue mitochondrial degradation. Moreover, enlarged lysosomes were observed, though these still possess degradative potential to mediate starvation-induced or PRKN-dependent mitophagy. Mass spectrometry analysis indicates that several glycolytic enzymes are activated in response to GAKi treatment, which may indicate that more fundamental metabolic changes are occurring that alter the cellular degradation of mitochondria.

PRKCD is a member of the large PKC kinase family and belongs to the subgroup of novel PKCs (nPKCs) including PRKCE, PRKCH and PRKCQ that are all activated with DAG independent of Ca^{2+}. Whilst we have primarily focused upon PRKCD due to its prominent mitochondrial localisation, it is interesting to note that all nPKCs reduced DFP-induced mitophagy to varying extents, suggesting DAG and PKCs play a prominent role in the regulation of mitophagy. Usage of a pan-PKC inhibitor consistently gave a stronger and more robust inhibition of DFP-induced mitophagy, indicating that several isoforms could play a role or serve redundant functions with one another. Treatment with the PKC inhibitor sotrastaurin led to a significant inhibition in the recruitment of early autophagy markers, thereby reducing mitophagosome formation.

Formation of mitochondrial DAG has previously been observed during oxidative stress induced by H_2O_2, which resulted in the recruitment of Protein Kinase D1 (PKD1) to mitochondria[45]. Recent data in mice have also implicated PKD1 in the regulation of mitochondrial depolarisation and is itself regulated by PRKCD in the activation loop at S738/S742, it is tempting to speculate that PKD1 might also be involved in DFP-induced mitophagy [46]. Another intriguing detail is that PKD1 can bind to AKAP13, another identified regulator of mitophagy in our screen [47]. The formation of mitochondrial DAG could therefore be a key step in the regulation of DFP-dependent mitophagy. DAG can be formed from phosphatidic acid by phosphatidic acid phosphohydrolases, such as the Lipin family of

444 proteins. Interestingly, Lipin-1 deficiency is associated with accumulation of mitochondria combined
445 with morphological abnormalities [48]. Additionally, Lipin-1 depletion was found to reduce the level of
446 PKD1 phosphorylation with a subsequent decrease in VPS34 mediated PtdIns(3)P formation [48].
447 Further examination of PKD1 regulation may therefore be important for studying the role of PKCs in
448 DFP-induced mitophagy.

449 Interestingly, neither GAK nor PRKCD inhibition was able to modulate PRKN-mediated mitophagy.
450 This adds further evidence that the machinery required for PRKN-dependent and independent
451 mitophagy pathways are fundamentally different. Tantalisingly, both *c.elegans* and *d.rario* models
452 indicate that basal mitophagy (along with DMOG-stimulated in zebrafish experiments) can be
453 regulated by these kinases as opposed to stress-induced mitophagy, such as that regulated by PRKN.
454 By looking at the hindbrain region of zebrafish, showing the highest expression of Prkcd, we observed
455 a significant reduction in the level of mitophagy upon depletion of prkcda and prkcdb and
456 impairment of locomotory responses. This may be due to deterioration of hindbrain locomotory
457 neurons as a consequence of impaired mitophagy or may be associated with an anxiety-like response
458 (thought to be triggered in zebrafish due to light changes) noted previously in mice to be impaired
459 with PRKCD depletion[49].

460 To conclude, this initial screen of lipid-binding proteins in DFP-induced mitophagy identified two
461 lipid-binding kinases that have been validated by functional characterisation and confirmation in
462 higher organisms. This highlights the importance of protein-lipid interactions and provides a strong
463 initial basis for further investigation into the molecular mechanisms of mitophagy.

464

Materials and Methods

Materials

Lysotracker Red DND-99 (L7528) was from ThermoFisher Scientific. Antimycin A (A8674), DFP (379409), DMOG (D3695), SGC-GAK-1 (GAKi, SML2202), SGC-GAK-1N (GAKc, SML2203) and Q-VD-OPh (SML0063) were from Sigma Aldrich. Bafilomycin A1 (BML-CM110), CCCP (BML-CM124) were from Enzo Life Sciences. Enzastaurin (S1055), Oligomycin A (S1478), and Sotrastaurin (S2791) were from Selleckchem. MRT68921 (1190379-70-4) and VPS34-IN1 (1383716-33-3) were from Cayman Chemical. IVAP1966 (12g) and IVAP1966 (12i) were gratefully received from the lab of Prof. Piet Herdewijn [21]. HY-19764 was gratefully received from the structural genomics consortium [22]. Bradford reagent dye (#5000006) was from Bio-Rad. 1,4-dithiothreitol (DTT, #441496P) was from VWR. Complete EDTA-free protease inhibitors (#05056489001) and phosphatase inhibitors (#04906837001) were from Roche.

Cell Lines, Maintenance and Induction of Mitophagy

U2OS FlpIN TRex cells with stable dox-inducible expression of MLS-EGFP-mCherry (referred to as IMLS cells) [11] were grown and maintained in a complete medium of Dulbecco's Modified Eagle Medium (DMEM – Lonza 12-741F) supplemented with 10% v/v foetal bovine serum (FBS – Sigma Aldrich #F7524) and 100 U/ml Penicillin + 100 µg/ml Streptomycin (ThermoFisher Scientific #15140122) in a humidified incubator at 37°C with 5% CO_2. U2OS IMLS cells with stable expression of PRKN were generated by cloning of PRKN into a pLenti-III-PGK viral expression vector that was co-transfected into 293FT cells with psPAX2 and pCMV-VSVG to generate lentiviral particles, which were transduced into U2OS IMLS cells and positive cells selected with puromycin (Sigma #P7255).

Mitophagy was typically induced utilising 1 mM DFP by addition to cell culture media for 24 h. In the case of PRKN overexpression, CCCP was used at 20 µM for 16 h or a combination of Oligomycin and Antimycin A (10µM and 1µM respectively) for 16 h. In the case of PRKN-dependent mitophagy

experiments, the pan-caspase inhibitor Q-VD-OPh [50] was included to reduce cell death and improve imaging quality, in accordance with previous papers studying PRKN-dependent mitophagy [51].

Imaging and Image Analysis

The initial siRNA screen, secondary siRNA screen and other experiments where indicated were carried out utilising an AxioObserver widefield microscope (Zen Blue 2.3, Zeiss) with a 20x objective (NA 0.5). Relevant channels were imaged using a solid-state light source (Colibri 7) and multi-bandpass filter (BP425/30, 524/50, 688/145) or individual filters. The tertiary siRNA screen was carried out utilising an ImageXpress Micro Confocal (Molecular Devices) using a 20x objective (NA 0.45). Confocal images were taken with a LSM710 microscope or LSM800 (Zebrafish experiments) microscope (Zen Black 2012 SP5 FP3, Zeiss) utilising a 63x oil objective (NA 1.4) combined with a laser diode (405nm), Ar-Laser Multiline (458/488/514nm), DPSS (561nm) and HeNe-laser (633nm) for relevant fluorophore acquisition.

Identification of relevant structures by image analysis was determined using CellProfiler software (v2.8.0, The Broad Institute) [52]. In the case of IMLS cell analysis for mitophagy, red only structures were identified by dividing the red signal by green signal per pixel following background noise reduction and weighting of the red signal to match that of the green signal in non-mitophagy inducing controls. By this method a value of ~1 indicates “yellow” networked mitochondria and values <1 represent mitochondria that have a stronger red signal than green signal. Values of <0.5 were taken to represent true red structures, regions that are therefore twice as bright for red than green.

Zebrafish Maintenance and *in situ* hybridisation (ISH)

Wild-type zebrafish (AB strain) and transgenic tandem-tagged mitofish (TT-mitofish)[11] were housed at the zebrafish facility at the Centre for Molecular Medicine Norway (AVD.172) using standard practices. Embryos were incubated in egg water (0.06 g/L salt (Red Sea)) or E3 medium (5 mM NaCl, 0.17 mM KCl, 0.33 mM CaCl2, 0.33 mM MgSO4, equilibrated to pH 7.0). Embryos were held at 28 °C in an

514 incubator following collection. Experimental procedures followed the recommendations of the
515 Norwegian Regulation on Animal Experimentation ("Forskrift om forsøk med dyr" from 15.jan.1996).
516 All experiments conducted on wild-type zebrafish and transgenic tandem-tagged mitofish larvae were
517 done at 5 dpf or earlier.

518 Whole-mount ISH for *prkcda* and *prkcdb* were performed as previously described using digoxigenin-
519 labelled riboprobes[53]. Primer sequences for sense and antisense probes are described in
520 Oligonucleotide Primers/Probes

521 Appendix 2.

522 **Screening Library**

523 Human targets for the siRNA library were identified by using the ExPASY PROSITE sequence motif
524 database identifier for human proteins containing true-positive identified lipid binding domains.
525 These included C1 domains (ID: PS50081), C2 domains (ID: PS50004), ENTH (ID: PS50942), PH Domain
526 (ID: PS50003), PX Domain (ID: PS50195), FYVE domain (PS50178), GRAM or PROPPIN (SVP1 family)
527 domains (No ID). This list was cross-checked against several previously published U2OS cell line
528 proteomes (determined by mass spectrometry) and proteins not observed to be expressed in U2OS
529 cells were removed [15,16]. See Appendix 1 for a full list of siRNA targets.

530 **siRNA knockdown**

531 The primary screen was carried out using a pooled siRNA approach with three Silencer Select siRNA
532 oligonucleotides targeting each gene at 2.5nM final concentration each (7.5nM final). For
533 transfection, 125µl of OptiMEM (Thermofisher Scientific #31985070) containing 100 ng/ml
534 Doxycycline (Clontech #631311) and 0.1 µl RNAiMAX per pmol siRNA (Thermofisher Scientific
535 #13778150) was added to each well of an Ibidi 96-well µ-plate (Ibidi #89626). After 5 mins at room
536 temperature (RT), 25 µl of 75 nM siRNA (pooled) diluted in OptiMEM was added per well and
537 incubated a further 15 mins at RT. U2OS IMLS cells were trypsinised and resuspended in complete
538 media before centrifugation at 300 x g for 5 mins at RT. Media was removed and cells resuspended in

OptiMEM to 2x10^5 cells/ml. 100 µl of cells were added per well and samples were incubated for 16 h at 37°C. The media was then removed and changed to complete media for a further 24 h before the media again was changed to complete media ± 1mM DFP and incubated for 24h to induce mitophagy. Control wells with BafA1 treatment were dosed 2h prior to fixation. At the end of the experiment, samples were washed once in PBS and then fixed in 3.7% PFA, 200 mM HEPES pH 7 for 15mins /37°C. PFA was then quenched by washing twice and incubating a further 15mins in DMEM + 10mM HEPES pH 7. Wells were then washed twice with PBS and then incubated in PBS + 2 µg/ml Hoechst to stain nuclei for a minimum of 1h prior to imaging. Images were obtained on a Zeiss AxioObserver widefield microscope with a 20x objective acquiring a minimum of 35 fields of view per treatment. Analysis of red only punctate structures was carried out utilizing CellProfiler from a minimum of 1000 cells per condition per replicate.

Identification and plotting of protein-protein interactome (PPI) networks

PPI represents the physical interaction among a set of proteins. PPI was obtained from Biological General Repository for interaction Datasets (BioGRID) version BIOGRID-ORGANISM-3.5.185.mitab[54] (compiled April 25th 2020) containing non-redundant and curated interactions. The networks were visualized using Cytoscape (v3.8.0) [55], we considered only the connected component of these seed networks for statistical and functional analysis. Functional and pathway analysis of connected components of interaction network was performed by ShinyGO[56]. We only considered GO terms for cellular component, molecular functions and biological process with significant p-value and enrichment values. Graphs were plotted using R package ggplots.

RNA Isolation, cDNA synthesis and qPCR

For quantifying knockdown in the secondary deconvolution siRNA screen, RNA was isolated and cDNA generated from transfected U2OS cells using *Power* SYBR Green Cells-to-C_T kit (ThermoFisher Scientific #4402955) as per manufacturer's instructions.

For other experiments, RNA was isolated from cells or zebrafish (~50 embryos per sample) using Trizol reagent (ThermoFisher Scientific #15596026). cDNA was synthesised from RNA using Superscript III reverse transcriptase (ThermoFisher Scientific #18080085) according to manufacturer's instructions. Amplification was performed with KAPA SYBR FAST qPCR Kit using a CFx96 real-time PCR system (Bio-Rad) using primers designed to amplify target genes as indicated in Oligonucleotide Primers/Probes

Appendix 2 following normalisation of transcript levels to TATA-box-binding protein (TBP – cell samples) or β-actin (zebrafish samples) using the $2^{-\Delta\Delta Ct}$ method.

Western Blotting

For western blotting experiments, cells were treated as indicated in figure legends prior to moving onto ice and washing twice with cold PBS. Cells were lysed on ice in NP-40 lysis buffer [50mM HEPES pH 7.4, 150mM NaCl, 1mM EDTA, 10% (v/v) Glycerol, 0.5% (v/v) NP-40 + 1mM DTT, 1x Phosphatase inhibitors and 1x Protease inhibitors fresh] and incubated 5 mins prior to collecting. For zebrafish samples, embryos were collected at 3 dpf and lysed in RIPA buffer [50 mM Tris-HCl pH 8, 150 mM NaCl, 5 mM EDTA, 1 % NP-40, 0.5 % Sodium deoxycholate, 0.1 % SDS, 1x protease inhibitor cocktail], approximately 20-30 embryos were used per gel lane.

Samples were clarified by centrifugation at 21000 x g / 4 °C / 10 mins and supernatant retained. Protein levels were quantified by Bradford assay (Bio-Rad #5000006) relative to a BSA standard. Samples were normalised and added to loading sample [1x = 62.5mM Tris pH 6.8, 10% (v/v) Glycerol, 2% (w/v) SDS, 0.005% (w/v) Bromophenol Blue] to achieve 30µg-50µg of protein per lane. Samples were ran by acrylamide gel and transferred to PVDF (350mA/50mins). Samples were blocked in TBS Odyssey Blocking Buffer (Li-Cor #927-50000) for 30mins/RT before incubation overnight at 4°C with primary antibodies (TBS blocking buffer + 0.2% Tween). Membranes were washed 3x10 mins in TBST before secondary antibody incubation (TBS blocking buffer + 0.2% Tween + 0.01% SDS) for 1h.

Membranes were washed 3x 10min with TBST before a final wash in TBS only and membrane imaging.

Antibodies

Primary antibodies targeting ATG13 (#13468, Clone E1Y9V), AMPK P-T172 (#2535), β-Actin (#3700, Clone 8H10D10), BNIP3 (#44060, Clone D7U1T), BNIP3L (#12396, Clone D4R4B), COXIV (#4850, Clone 3E11), PDH (#2784), PRKCD (#9616, D10E2), PRKCD P-S663 (#9376), LC3B (Western blotting only, #3868, Clone D11), ULK1 (#8054), ULK1 P-S555 (#5869), ULK1 P-S757 (#6888, Clone D1H4) were from Cell Signaling Technology. FUNDC1 (#Ab74834), GAK (#Ab115179, Clone 1C2), NIPSNAP1 (#Ab67302), MTCO2 (#Ab110258, Clone 12C4F12) and WIPI2 (#Ab105459, Clone 2A2) were from Abcam. ATG13 P-S318 (#600-401-C49S) was from Rockland. HIF1α (MAB1536-SP, Clone 241809) was from R&D Systems. LAMP1 (sc-20011, Clone H4A3) was from Santa Cruz Biotechnology. α-Tubulin (T5168, Clone B-5-1-2) was from Sigma Aldrich.

Secondary antibodies for western blotting are indicated in the source data file, these included anti-rabbit (Starbright Blue, Bio-Rad, 12004161) (DyLight 800, ThermoFisher Scientific, SA5-10044) (DyLight 680, ThermoFisher Scientific, SA5-10042) or anti-mouse (Starbright Blue, Bio-Rad,12004158) (DyLight 680, ThermoFisher Scientific, SA5-10170) or anti-tubulin (hFAB Rhodamine, Bio Rad, 12004166). Secondary antibodies for immunofluorescence were anti-rabbit Alexa Fluor-594 (Invitrogen, A11058), Alexa Fluor-647 (ThermoFIsher Scientific, A21245) or anti-mouse Alexa Fluor-647 (ThermoFisher Scientific, A21236).

Phos-Tag Gels

Phos-tag acrylamide gels were prepared in line with manufacturer's instructions. Briefly, 8% resolving poly-acrylamide gels were prepared containing 25µM Phos-tag reagent (Wako Chemicals #AAL-107) and 50µM $MnCl_2$ [26]. Samples to be ran for analysis were diluted in loading sample containing 10 mM $MnCl_2$. Acrylamide gels were ran at 40 mA until complete and washed 3x10 min/RT in 1x transfer buffer (48mM Tris, 39mM Glycine, 0.0375% (w/v) SDS) + 10mM EDTA followed by 1x10min in 1x

transfer buffer. Samples were then transferred to PVDF at 350mA / 50min and treated as noted earlier for western blot samples.

PFA Fixation, antibody staining and imaging

Cells to be imaged were seeded onto glass coverslips 16h prior to treatments as indicated in figure legends. Following treatment, cells were washed once with PBS prior to addition of warmed fixation buffer (3.7% (w/v) PFA, 200mM HEPES pH 7.4) or for double tag IMLS cells (3.7% (w/v) PFA, 200mM HEPES pH 7) and incubated 15 mins at 37°C. Coverslips were washed twice and incubated 1x15 mins with DMEM + 10mM HEPES pH7.4 (IMLS = pH 7). Cells were then washed once with PBS and then permeabilised by incubation for 5 mins with permeabilisation buffer (0.2% (v/v) NP-40 in PBS). Cells were washed twice and then incubated 20 mins with IF blocking buffer (PBS + 1% (w/v) BSA) to block the samples. Coverslips were then incubated 1 h / 37 °C with primary antibodies diluted in IF blocking buffer before washing 3x10 mins in IF blocking buffer. Coverslips were then incubated 30 mins / RT with appropriate secondary antibodies. Finally, samples were washed 3x10 mins in IF blocking buffer prior to mounting on to coverslides with ProLong Diamond Antifade Mountant with DAPI (ThermoFisher Scientific #P36962). Slides were allowed to cure overnight before imaging with either a Zeiss AxioObserver widefield microscope (20x) or Zeiss LSM 800 confocal microscope (60x).

Citrate Synthase Assay

To biochemically quantify mitochondrial abundance, we assayed citrate synthase activity from cell lysates. Briefly, U2OS cells were grown and subject to treatments as described in figure legends, cells were then washed twice with PBS on ice before lysis [50 mM HEPES pH 7.4, 150 mM NaCl, 1 mM EDTA, 10 % Glycerol, 0.5 % NP-40, 1 mM DTT, 1x Phosphatase inhibitors, 1x Protease inhibitors]. Cell lysates were clarified by centrifugation at 21000 x g / 10 min / 4 °C and supernatants retained. Protein concentration was determined by Bradford assay. To determine citrate synthase activity 1 µl of protein lysate was added to 197 µl of CS assay buffer [100 mM Tris pH 8, 0.1 % Triton X-100, 0.1 mM Acetyl CoA, 0.2 mM DTNB [5,5'Dithiobis(2-nitrobenzoic acid)]) in a multi well plate. At the

assay start point, 2 µl of 20 mM Iodoacetamide was added per well and incubated at 32 °C and reactions monitored at λ_{Abs}=420 nm for 30 min in a FLUOstar OPTIMA (v2.20R2, BMG Labtech) plate reader and compared to iodoacetamide null controls. The $\Delta \lambda_{Abs}$ was plotted and the reaction rate determined across the linear range before saturation. The reaction rate was then normalised to the protein concentration and plotted relative to the control.

Correlative Light Electron Microscopy (CLEM)

For CLEM, U2OS IMLS cells were grown on photo-etched coverslips (Electron Microscopy Sciences, Hatfield, USA). The next day, cells were treated with DFP (1mM) ± GAKi (10 µM) for 24 h. Cells were then fixed in 4 % formaldehyde, 0.1 % glutaraldehyde/0.1 M PHEM (60 mM PIPES, 25 mM HEPES, 2 mM $MgCl_2$, 10 mM EGTA, pH 6.9), for 1 h. The cells were mounted with Mowiol containing 2 µg/ml Hoechst 33342 (Sigma-Aldrich). Mounted coverslips were examined with a Zeiss LSM710 confocal microscope with a Zeiss plan-Apochromat 63x/1.4 Oil DIC III objective. Cells of interest were identified by fluorescence microscopy and a Z-stack was acquired. The relative positioning of the cells on the photo-etched coverslips was determined by taking a DIC image. The coverslips were removed from the object glass, washed with 0.1 M PHEM buffer and fixed in 2 % glutaraldehyde/0.1 M PHEM for 1h. Cells were post fixed in osmium tetroxide and uranyl acetate, stained with tannic acid, dehydrated stepwise to 100% ethanol and flat-embedded in Epon. Serial sections (~100-200nm) were cut on an Ultracut UCT ultramicrotome (Leica, Germany), collected on formvar coated slot-grids. Samples were observed in a Thermo Scientific™ Talos™ F200C microscope and images were recorded with a Ceta 16M camera. For tomograms, single-tilt image series were recorded between -60° and 60° tilt angle with 2° increment. Single axis tomograms were computed using weighted back projection and, using the IMOD software package version 4.9[57].

Mitochondrial Enrichment

Cells to be enriched for mitochondria were grown and treated as noted in figure legends. Cells were then moved to ice and washed twice with ice cold PBS. 1 ml of mito fractionation buffer (5 mM Tris-

HCl pH 7.5, 210 mM Mannitol, 70 mM Sucrose, 1 mM EDTA pH 7.5, 1 mM DTT, 1x protease and phosphatase inhibitors) was added per 10 cm dish and scraped to collect cells. A "cell homogenizer" (Isobiotec) was utilised with a 16 µm clearance ball and prepared by passing through 1 ml of mito fractionation buffer. Cell solution was collected in a 1 ml syringe and passed through the cell homogenizer 9 times. The resulting mix was centrifuged 500 x g / 4°C / 5 mins to pellet unbroken cells and nuclei. The supernatant was taken, and a small sample retained as post nuclear supernatant, the remaining was centrifuged at 10000 x g/4°C/ 10 mins to pellet mitochondria. The supernatant was removed to waste, and the pellet resuspended in 500 µl mito fractionation buffer and 10000 x g/4 °C/10 mins centrifugation step repeated. The supernatant was removed once more, the pellet represents enriched mitochondria that could be added directly to protein loading sample for downstream western blotting.

Mitochondrial Classifier

Cellular mitochondria were classified as tubular or fragmented by implementing an image classified utilising CellProfiler Analyst (v2.2.1, The Broad Institute). Classifications were determined by using siDRP1 and siOPA1 treated cells as positive controls for fragmented and hyperfused phenotypes respectively. Classifier was trained on the EGFP fluorescent images and with a confusion matrix of >0.90 for each phenotype.

Crystal Violet Staining

U2OS cells were seeded into 96-well plates in triplicate at $2x10^4$ cells per well and incubated overnight in complete media. Cells were then treated for 24 h with indicated compounds and doses, utilising puromycin as a positive control. Following treatment, cell media was removed and cells washed twice with a gentle stream of water. This was then removed and 100 µl of staining solution (0.5% (w/v) crystal violet, 20% methanol) added and incubated 20 min / RT with gentle rocking. Wells were washed 4x with water, all liquid removed and left overnight to air dry. Then 200µl per well of 100% methanol for 20min/RT was added with gentle rocking and sample absorbance read at OD_{570}.

687 Sample values were adjusted by no-well control (blank) wells and viability determined by
688 normalisation to an untreated control.

689 **Quantification of mitophagy in *C. elegans*.**

690 The strain used to monitor mitophagy process in *C. elegans* was IR2539:
691 *unc-119(ed3);Ex*[$_{pmyo-3}$TOMM-20::Rosella;unc-119(+)]. Standard procedures for *C. elegans* strain
692 maintenance were followed. Nematode rearing temperature was kept at 20°C. For RNAi experiments
693 worms were placed on NGM plates containing 2 mM IPTG and seeded with HT115(DE3) bacteria
694 transformed with either the pL4440 vector or the gakh-1 RNA construct for two generations.
695 Synchronous animal populations were generated by hypochlorite treatment of gravid adults to
696 obtain tightly synchronized embryos that were allowed to develop into adulthood under appropriate,
697 defined conditions. Progeny of these adults were tested on adult day 2. We performed imaging of
698 mitophagy process in *C. elegans* based on the methods we had established [58–60]. Briefly, worms were
699 immobilized with levamisole before mounting on 2% agarose pads for microscopic examination using
700 EVOS Imaging System. Images were acquired as Z-stacks under the same exposure. Average pixel
701 intensity values and frequency of GFP/DsRed puncta were calculated by sampling images of different
702 animals. The calculated mean pixel intensity for each animal in these images was obtained using FIJI.

703 **CRISPR/Cas9 genome editing in zebrafish and microinjections**

704 To generate *prkcda* and *prkcdb* knock-out embryos, we utilised CRISPR/Cas9 as described earlier (Jao
705 et al., 2013). Potential gRNA target sites were identified using the online web tool CRISPR Design
706 (http://CRISPR.mit.edu) or CHOPCHOP (http://chopchop.cbu.uib.no/index.php) (Montague et al.,
707 2014). Genomic DNA sequences retrieved from Ensembl GRCz10 or z11
708 (http://uswest.ensembl.org/Danio_rerio/Info/Index) were used for the target site searches. Three
709 guide RNAs were designed each for *prkcda* and *prkcdb* respectively, based on predictions from the
710 aforementioned web programs. All sgRNAs were prepared by *in vitro* transcription of double-stranded
711 deoxyoligonucleotide templates as described previously [61]. Cas9 nuclease (EnGen Cas9 NLS, NEB) was

combined with an equimolar mixture of 3x sgRNA's (or 6x for *prkcd_ab* DKO) and incubated for 5-6 minutes at room temperature. After incubation, the mixture was immediately placed back on ice, until pipetted into the capillary needle used for microinjection and then approximately 1 nl of 5 µM sgRNA:Cas9 complex was microinjected into the cytoplasm of one celled stage zebrafish embryo.

Oligonucleotides used for sgRNA synthesis are listed in Oligonucleotide Primers/Probes Appendix 2, a universal primer was used with individual sgRNA primers (5'AAAAGCACCGACTCGGTGCCACTTTTTCAAGTTGATAACGGACTAGCCTTA TTTTAACTTGCTATTTCTAGCTCTAAAAC'3).

Zebrafish Locomotor Assay

Larval motility was monitored using the ZebraBox and Viewpoint software (v3.10.0.42, Viewpoint Life Sciences Inc) under infrared light. At 5 days post fertilization (dpf), larvae were singly placed in 48-well plates with 300 µl of fish water per well, followed by incubation at 28.5 °C on a normal light cycle overnight. All experiments were completed in a quiet room at 5 dpf between 10 AM and 2 PM. Larvae were allowed to acclimate in the ZebraBox measurement apparatus for 2 h before recording. Larvae were then exposed to alternating cycles of infrared light and dark, every 30 min as described [63]. Larval locomotion was tracked with the Viewpoint software. Motility was defined as tracks moving less than 10 cm/s, but more than 0.1 cm/s.

Zebrafish Mitophagy cryosectioning and confocal microscopy

Zebrafish mitophagy experiments were conducted on tt-mitofish with relevant prkcd_a/b KO lines as described above. To examine mitophagy, zebrafish larvae were treated with DMOG or control for 24 h. At experimental end-points, larvae were washed once in embryo water and fixed with 3.7% PFA (in HEPES, pH 7-7.2) at 4 °C overnight. Post fixation, larvae were washed three times in PBS. The larvae were then cryopreserved in a 2 mL tube in increasing amounts of sucrose in 0.1 M PBS with 0.01 % sodium azide. Cryopreservation was done first in 15 % sucrose solution for 1 hour at RT or up until the larvae drops to the bottom of the tube and then in 30% sucrose solution at 4 °C overnight with gentle

737 shaking. Cryopreserved larvae were oriented in a cryomold (Tissue-Tek Cryomold, Sakura, Ref: 4565)
738 with optimal cutting temperature compound (OCT compound) (Tissue-Tek Sakura, Ref: 4583). Larvae
739 were oriented with the ventral side down and additional OCT was added to fill the mold and frozen
740 down on dry ice. A solid block of OCT with couple of larvae oriented in the desired way, was taken out
741 from the mold and 12 µm coronal slices were sectioned on the cryostat (Thermo Scientific). Sections
742 were collected on Superfrost Plus glass slides (Thermo Scientific, Ref: J1800AMNZ) and kept at RT for
743 at least 2 h to firmly tether slices onto the glass slide.

744 The pH of all solutions and buffers used were 7-7.2. Slides were rehydrated three times in PBST (0.1 %
745 Tween 20 in 1X PBS) at room temperature for 3 minutes each. Area of interest was circled by a
746 hydrophobic PAP pen (Abcam, ab2601) and the slides were placed in a humidified chamber to avoid
747 drying out. 100-200 µl of 1 µg/ml Hoechst solution was gently pipetted onto the slides and incubated
748 for 30 mins at RT. Post incubation, slides were washed 3 times in PBST for 5 minutes each and mounted
749 using ProLong Diamond Antifade Mountant (Invitrogen, P3696). Coverslips were carefully placed over
750 the sections. Confocal images were obtained using an Apochromat 20x/0.8 or 63x/1.2 oil DIC objective
751 on an LSM 800 microscope (Zeiss). Red puncta were counted manually from hind-brain regions.

752 **Mass Spectrometry**

753 Sample Preparation

754 Cells were dissolved in RIPA buffer and further homogenized with a sonicator (30 sec x 3 times with 30
755 sec interval) and insoluble material was removed by centrifugation. Protein concentrations were
756 estimated by BCA assay (Pierce). For each replicate, 600 µg of protein samples for phosphoproteomics
757 and 30 µg for whole cell lysate proteomics were reduced and alkylated and further digested with
758 trypsin by FASP (Filter aided sample preparation) method. Digested peptides were transferred to a
759 new tube, acidified and the peptides were de-salted using Oasis cartridges for STY peptides
760 enrichments. Phosphorylated peptides enrichment was performed based on TiO_2 [64]**.** Enriched peptides
761 fractions were de-salted by C_{18} stage tips.

LC-MS/MS:

Peptide samples were dissolved in 10 µl 0.1 % formic buffer and 3 µl were loaded for MS analysis. The Ultimate 3000 nano-UHPLC system (Dionex, Sunnyvale, CA, USA) connected to a Q Exactive mass spectrometer (ThermoElectron, Bremen, Germany) equipped with a nano electrospray ion source was used for analysis. For liquid chromatography separation, an Acclaim PepMap 100 column (C18, 3 µm beads, 100 Å, 75 µm inner diameter) (Dionex, Sunnyvale CA, USA) capillary of 50 cm bed length was used. A flow rate of 300 nL/min was employed with a solvent gradient of 3-35 % B in 220 mins, to 50 % B in 20 min and then to 80 % B in 2 min. Solvent A was 0.1 % formic acid and solvent B was 0.1 % formic acid/90% acetonitrile.

The mass spectrometer was operated in the data-dependent mode to automatically switch between MS and MS/MS acquisition. Survey full scan MS spectra (from m/z 400 to 2000) were acquired with the resolution R = 70,000 at m/z 200, after accumulation to a target of 1e6. The maximum allowed ion accumulation times were 100 ms. The method used allowed sequential isolation of up to the ten most intense ions, depending on signal intensity (intensity threshold 1.7e4), for fragmentation using higher collision induced dissociation (HCD) at a target value of 10,000 charges and a resolution R = 17,500. Target ions already selected for MS/MS were dynamically excluded for 30 sec. The isolation window was m/z = 2 without offset. The maximum allowed ion accumulation for the MS/MS spectrum was 60 ms. For accurate mass measurements, the lock mass option was enabled in MS mode and the polydimethylcyclosiloxane ions generated in the electrospray process from ambient air were used for internal recalibration during the analysis.

Data Analysis:

Raw files from the LC-MS/MS analyses were submitted to MaxQuant (v1.6.1.0) software for peptide/protein identification[65]. Parameters were set as follow: Carbamidomethyl (C) was set as a fixed modification; protein N-acetylation and methionine oxidation as variable modifications and PTY. A first search error window of 20 ppm and mains search error of 6 ppm was used. Minimal unique peptides

were set to one, and FDR allowed was 0.01 (1 %) for peptide and protein identification. The Uniprot human database was used. Generation of reversed sequences was selected to assign FDR rates. MaxQuant output files (proteinGroups.txt for proteomic data and STY(sites).txt for phosphoproteomic data) were loaded into the Perseus software[66]. Identifications from potential contaminants and reversed sequences were removed and intensities were transformed to log2. Identified phosphorylation sites were filtered only for those that were confidently localized (class I, localization probability ≥ 0.75). Next, proteins identified in two out three replicates were considered for further analysis. All zero intensity values were replaced using noise values of the normal distribution of each sample. Protein or STY abundances were compared using LFQ intensity values and a two-sample Student's T-test (permutation-based FDR correction (250 randomizations), FDR cut-off: 0.05, S0: 0.1).

The complete datasets have been uploaded to ProteomXchange.

Statistics and Significance

Experimental values were used for statistical analysis using Prism (v8.0.1) where indicated using analyses and post-hoc tests as indicated in figure legends. All data values come from distinct samples. Where shown **** = p>0.0001, *** = p >0.001, ** = p>0.01, * = p > 005 or n.s = not significant.

ACKNOWLEDGEMENTS

We would like to thank Coen Campersteijn for assistance with live cell imaging. We would also like to thank the Simonsen lab for their support and critical discussion throughout.

This work was supported by the Norwegian Cancer Society (Project: 171318) and the Research Council of Norway through its Centres of Excellence funding scheme (Project: 262652) and FRIPRO grant (Project: 221831).

AUTHOR CONTRIBUTIONS

Experimental planning, data analysis and writing of the manuscript were performed by M.J.M and A.S with input from all authors. B.J.M carried out *D.rario* experiments, Seb.S carried out CLEM experiments. Y.A and E.F carried out *C.elegans* experiments. Sac.S and J.W prepared and ran samples for MS analysis. Sak.S carried out analysis of interaction networks. A.H.L generated the IMLS cell line. M.J.M, L.T.M, M.Y.W.N.G and L.R.dlB performed all remaining experiments.

AUTHOR DECLARATIONS

M.J.M is now an employee of AstraZeneca plc.

DATA AVAILABILITY

All data is available upon reasonable request. Source data for quantitative figures and supplementary figures is provided as supplementary information. Proteomics Data has been uploaded to PRIDE.

APPENDICES

siRNA Targets List

Appendix 1 – siRNA Targets

Gene Name	RefSeq	Lipid Binding Domain(s)	Sense siRNA			siRNA ID			Primary Screen	
			Oligo #1	Oligo #2	Oligo #3	Oligo 1	Oligo 2	Oligo 3	Average (fold)	SEM
ABR	NM_001092	PH, C2	GCGAAGAGAUCUACAUUAAtt	CGGCUAUUUUGUCAGCAAAtt	CGGACGUGAUUGAGAUGAAtt	s876	s877	s878	**-0.14**	0.09
AKAP13	NM_006738	PH, C1	GCAUAUUGCUUGUAACUCAtt	GGAAGAAGCUUGUACGUGAtt	GGAUAAUAGACAGCAAGUUtt	s680	s681	s682	**-0.74**	0.04
ANKFY1	NM_016376	FYVE	GGACUUCAUUUGAUGAGAAtt	GAAACUAGCAAAUCGGUUUtt	GUACAGCGAUCUGAAGAUAtt	s28198	s28199	s28200	**+0.15**	0.10
ARAF	NM_001654	C1	CGAGAUCUCAAGUCUAACAtt	GUGUUGACAUGAGUACCAAtt	UGCACAAUUUUGUACGGAAtt	s575	s576	s577	**+0.78**	0.12
ARHGAP29	NM_004815	C1	GCAUAGGUGUUGUUGAUCAtt	GACCAAGGCUAAAACGAAUtt	GGUCAACUCUCUACUGAUAtt	s484	s485	s486	**+0.09**	0.05
Arhgap33	NM_178252	PX (atypical)	GGAAGACAUUCUUUGCUCUtt	GAGGUUCUGUUCAGCGAUAtt	GGCAUGAGUUUGAUAGUGAtt	s107439	s107440	s107441	**+0.22**	0.05
ARHGEF2	NM_004723	PH, C1	GGAUCUACCUGUCACUACUtt	CCAAGUACCCGUUACUCAUtt	GCUUACCUGCGGCGAAUUAtt	s17545	s17546	s17547	**-0.37**	0.02
Arhgef28	NM_012026	PH, C1	CGAUUUGGAUAUCAACUAUtt	CCGACUGCGUCUUAACGAAtt	GCUUCGCAGUCUUUCGUGAtt	s99834	s99835	s99836	**+0.10**	0.05
BRAF	NM_004333	C1	CAGAGGAUUUUAGUCUAUAtt	GCAUAAUCCACCAUCAAUAtt	CAGUUGUCUGGAUCCAUUUtt	s2080	s2081	s2082	**+0.01**	0.05
C2CD5	NM_014802	C2	GCUCGGAUGAAGUUACAGAtt	GGAAAUUUCCGGAAUCGUUtt	GCCUCAACCUGACUAAUCAtt	s19053	s19054	s19055	**+0.11**	0.08
CDC42BPA	NM_014826	PH, C1	GAUGGAAGAUGGAACGGUUtt	CCGCAAUCAUAGAUCAUGAtt	CCAUAUCUCUCGGUGUACAtt	s16098	s16096	s16097	**-0.10**	0.08
CDC42BPB	NM_006035	PH, C1	CGAGAACGGCAUAACGAGAtt	CACUCAACUCCAUCGAAUAtt	GGCUGAUCCUUUGCUAUGAtt	s18401	s18402	s18403	**+0.41**	0.14
CDC42BPG	NM_017525	PH, C1	GCAAGAUCAUGAACCACGAtt	GGAUGUGAACGGGCACAUUtt	CAAACUCCCUGAUUCCCUUtt	s30983	s30984	s30985	**-0.13**	0.07
CHN1	NM_001822	C1	CAUUGAAUGAUAUACGGUAtt	CAUUAUCACUGGUGCACUUtt	CUCUCUAUAUUGAAACCAAtt	s3016	s3017	s3018	**-0.48**	0.06
CIT	NM_007174	PH, C1	GGAAGGUGAUGACCGUCUAtt	CGUGGAUUCUUACGGAAGAtt	GAUUCUUACGGAAGACGUAtt	s21910	s21911	s21912	**+0.12**	0.06
CLINT1	NM_014666	ENTH	GCUCCUAGCUUACCUCAUAtt	GCACAAUUGAUGACACCAUtt	GAAUGUUAAAAGACAACAAtt	s18644	s18645	s18646	**+0.53**	0.12
CPNE1	NM_152925	C2 x2	GAAUCUAUGACAUAGACAAtt	CCAUGUCAGUGAUCAUUGUtt	GCUACGCUUUGGAAUCUAUtt	s17023	s17024	s17025	**+0.77**	0.12
CPNE2	NM_152727	C2 x2	GGACUGAGGUGAUCAAGUAtt	UGUUCACCGUUGGAAUAGAtt	CUACUGGACCGGGAUGUUAtt	s47982	s47983	s47984	**+1.32**	0.15
CPNE3	NM_003909	C2 x2	CCAUUAAGGUGGAGUGUUAtt	GGAUAAUAAGGAUCUAUUUtt	GCAUUACGAUUUCAGCUGAtt	s17005	s17006	s17007	**+0.30**	0.08

CPNE7	NM_153636	C2 x2	GGAUUACGACUCUCGAGGAtt	AGUAUGAGGUGUCCCAUGAtt	CAGCCGAACGAGUACCUGAtt	s25879	s25880	s25881	**+1.04**	0.16
DAB2IP	NM_138709	PH, C2	CGAUCUUUCCGGUCUGAUAtt	GCUGUGGACUCCAAACAGAtt	GAGCAUGAGUGGACCAACAtt	s237	s238	s239	**+0.97**	0.11
DGKA	NM_201554	C1 x2	GGAUCGUAAAAAUAGCAAAtt	GCAUCGCAGUGCUAAACAUtt	CCGGAGAAGUUCAACAGCAtt	s3911	s3912	s3913	**+0.26**	0.10
DYSF	NM_003494	C2 x7	GCGUGAACCCUGUAUGGAAtt	GGACCUCCCUUCAACAUCAtt	GGGUCGACCUAUUUCCGAAtt	s15788	s15789	s15790	**+0.64**	0.10
EEA1	NM_003566	FYVE	GCUAAGUUGCAUUCCGAAAtt	GCUGGAUAAUACAACUGCAtt	GCAAUCUAGUCAACGGAGAtt	s15969	s15970	s15971	**-0.06**	0.07
ENTHD1	NM_152512	ENTH	GCACAUAGAUGAAGCUGGAtt	CGAUCGCUAGAUUACAUGAtt	GAUUCAUGGUUGGAAAUCAtt	s45419	s45420	s45421	**+0.20**	0.14
EPN1	NM_013333	ENTH	AAUCCUUGGUGAUGAUUUUtt	GACUUUGACCGACUCCGCAtt	CAUCGUCCACAACUACUCAtt	s26712	s26713	s26714	**-0.32**	0.04
EPN2	NM_148921	ENTH	CGCUGUUGGAUUUAAUGGAtt	GGAAAACACCUGAGUCCUUtt	AGAGCGAGCUUUAAAACUAtt	s22639	s230616	s230617	**-0.15**	0.06
EPN3	NM_017957	ENTH	GACUCUCUGAGGUAGAAAAtt	CGUGUACAAGGCUCUAACAtt	CAACUACUCCGAGGCAGAAtt	s30052	s30053	s30054	**+0.26**	0.05
ESYT1	NM_015292	C2 x5	GGACUUGAACAUCAGCUAUtt	CCAUGAUCAUGGACUCCAUtt	GGGAAGGUGUUACAGGCUAtt	s23605	s23606	s23607	**+0.02**	0.06
Esyt2	NM_028731	C2 x3	GGAAACCACUUUUAGAGAUtt	GAGUAAGAUUCGAUACAAAtt	CAAAUCCUCUUGUCCAGAUtt	s78925	s78926	s78927	**-0.37**	0.05
FAM148C	XM_065166	C2	GUGUCUCUGCUCAAAGGUUtt	GCAAUGUGUUGACGCCCGAtt	GGAGGUGACAAGUCUUGGAtt	s43053	s195676	s195677	**-0.34**	0.05
FGD1	NM_004463	FYVE, PHx2	CCUUGGUGCUGUAUAUCUAtt	CAAGAUGUAUGGUGAGUAUtt	GCAAAAGGUGUUUCACAUUtt	s5121	s5122	s5123	**+0.19**	0.20
FGD2	NM_173558	FYVE, PHx2	AGAAGAAGAUCGUCCAGGAtt	UCGGUGACGUGAUCCAGAAtt	GGGCCGAACUGAAAUACGAtt	s48057	s48058	s48059	**+0.35**	0.20
FGD3	NM_033086	FYVE, PHx2	GAACUUUGACCGAGCCGUAtt	UCAUGGGCAUAUUCUCUAAtt	AGAGCUGAGUGGUAGCUUAtt	s40147	s40148	s40149	**+0.49**	0.14
FGD4	NM_139241	FYVE, PHx2	GAAGGAGACUAAUGAGCAAtt	CAACCACACCUCAACAAAAtt	GAAAGGAUUUGAUAAUGCAtt	s42476	s42477	s42478	**+0.18**	0.09
FGD5	NM_152536	FYVE, PHx2	GGAGGACAGUGCUUCAAGAtt	CGAAAGGUUUAGAAUCAGAtt	GACUAUUUAAACAACCUUUtt	s45682	s45683	s45684	**+0.08**	0.11
FGD6	NM_018351	FYVE, PHx2	GUCUGUCACCGUAUCGUCAtt	GAUGAGACUUUGACUAUAAtt	GAAGUUACCUCAUCCUAUUtt	s31503	s31504	s31505	**-0.18**	0.08
FYCO1	NM_024513	FYVE	CCUGCAAUUUGAUCAGAAAtt	GAGGCACAGUUAGACGAUAtt	CACUGACCGUGGAAAAGGAtt	s35794	s35795	s35796	**+0.16**	0.12
GAK	XM_001127411	C2-tensin type	GUCCGUCGCUAAUUAUGCAtt	CACCAGAAAUCAUAGACUUtt	CGAGGAAUACAACACCAAUtt	s5527	s5528	s5529	**-0.55**	0.02
GRAMD1A	NM_020895	GRAM	GGAGCGGCAUUGAAGACUAtt	GAAGUGACAUGUCUGAAGAtt	GAGGAGCUAUUGACAGACAtt	s33529	s33530	s33531	**+0.20**	0.06
GRAMD1B	NM_020716	GRAM	GAGAGUGAAUGUUACGUGAtt	CCAGUGCUAUGGGAACGAAtt	CUCUUAGAGUCCCAACAAAtt	s33112	s33113	s33114	**+0.68**	0.11
GRAMD1C	NM_017577	GRAM	CUGCUCGACUCAUCCCAAAtt	GAUUACUUCUAUACCGUGAtt	CCUACACUAUAGUCCUUAAtt	s29399	s29400	s29401	**+0.74**	0.07
GRAMD2	NM_001012642	GRAM	GGAUGUUCCCUUGGAGGAAtt	CAAAGAAUGCUGUCUAUGAtt	CGAGAAGGGAUAACACUGAtt	s47069	s47070	s47071	**-0.18**	0.03
GRAMD3	NM_023927	GRAM	GGACACCCAUAAUACUGAAtt	CGACCUUCUACAUGAGAUAtt	GAAAGCUCUUUGUAUCAGAtt	s35302	s35303	s35304	**-0.23**	0.04
GRAMD4	NM_015124	GRAM	GAAAUUGCCUUAUUGGAAAtt	CCUCCAAAGGAAGACCUGAtt	CCCAGAACCUUUUCGGGAAtt	s23148	s23149	s23150	**+0.52**	0.03
HECW1	NM_015052	C2	GGACAGCUGCAAUUCCGAUtt	GCUCCGCAAUUUCUACAGAtt	GAUGAGGUCUUGUCCGAAAtt	s22968	s22969	s22970	**+0.06**	0.07
HGS	NM_004712	FYVE	CGUCUUUCCAGAAUUCAAAtt	UGGAAUCUGUGGUAAAGAAtt	CACGGUAUCUCAACCGGAAtt	s17480	s17481	s17482	**+0.55**	0.22
HIP1	NM_005338	ENTH	CCACUUAAUUGAGCGACUAtt	GCAAAUCACAGAUCGAAGAtt	GAGCCUGUCUGAGAUAGAAtt	s6542	s6543	s6544	**-0.10**	0.04

HIP1R	NM_003959	ENTH	GGACCGAUGUCAACAACAUtt	GCAGGAAUGUUCUCGCACAtt	GAUUGUGAGCUGAAGCUUUtt	s17203	s17204	s17205	**+0.24**	0.06
HS1BP3	NM_022460	PX	AGAUGGACAUCUUGCAGUAtt	UGAGGAGUUUUACCAGAAAtt	GGUGAUACCCAGAAAACCAtt	s34647	s34648	s34649	**+0.46**	0.09
ITCH	NM_031483	C2	CGGGCGAGUUUACUAUGUAtt	GGAACUGCUGCAUUAGAUAtt	GGAAUACAUCAGAAUGGUAtt	s38163	s38164	s38165	**-0.38**	0.05
ITSN1	NM_003024	PH, C2	GCUCAACAUCUGUAGAUCAtt	CAAGAACUAUUCUUAUGCAtt	GAACGAAAGAUCAUAGAAUtt	s12793	s12794	s12795	**-0.47**	0.04
ITSN2	NM_147152	PH, C2	CAACGUAAGGAUAAGGAUAtt	GGAGUGAAGUAAAACGGGAtt	CUGGAUCUGUAUCACCUAUtt	s27052	s27053	s27054	**+0.66**	0.12
KIF16B	NM_024704	PX	CAACUGCGUUUCUUCGAAUtt	GAAUUAUGGUGACGUAGAAtt	CCAAUAUGUUUCGCUUUAAtt	s31080	s31081	s31082	**+0.24**	0.06
LRBA	NM_006726	PH-Beach	GGCGGUAUAUCUCCAGUAAtt	GCUCGUUCUGAGUCAUAUAtt	GGUUACGUGUUAUCUACAAtt	s2735	s2736	s2737	**-0.25**	0.07
LYST	NM_000081	PH-Beach	CCAAAUGACUUACUCGAAAtt	GCAACGGUGUUUCAUCACAtt	GCAUUAGCACUGCGAGUUAtt	s3028	s3029	s3030	**-0.40**	0.02
MTM1	NM_000252	GRAM	CAUUGAAGGGUUCGAAAUAtt	GGUACUUUCUUAUUCAACUtt	CUGUGAAUCUGCUCGAGAAtt	s9041	s9042	s9043	**+0.54**	0.05
MTMR1	NM_003828	GRAM	GCUUAUAGCUGCUACAAUUtt	GUUACUACAGGACCAUUAAtt	GGAUCACCUUUAUAGCUGUtt	s16718	s16717	s16719	**+0.00**	0.07
MTMR2	NM_016156	GRAM	GGACAUCGAUUUCAACUAAtt	CUCUGACUGUCACGAAUUAtt	GAGAGAAUCAUUACGAAAAtt	s17014	s17015	s17016	**-0.20**	0.11
MTMR3	NM_153050	FYVE	GCUGGACCCUUAUUACCGAtt	GGAACAUUCCUGUGCAACAtt	GGAUGGGUUUUGAUAUGAAtt	s17011	s17012	s17013	**+0.02**	0.09
MTMR4	NM_004687	FYVE	CGUACAUCCAGUGACCCUAtt	GGAUUUUGGGCACAAGUUUtt	GCAACACCUCUGAUCCUGAtt	s17383	s17384	s17385	**+0.07**	0.07
MYO9A	NM_006901	C1 x2	GGAUAGUUUUUCGAAUUAAtt	GCUCUUACUUUGGAUAUCAtt	GUAAUAGAGAGUAAUCGAAtt	s9220	s9221	s9222	**-0.03**	0.05
MYO9B	NM_004145	C1	CGAUGUACUCUGUCCCGAAtt	GGAACUACCAGAUCGGGAAtt	GAAAAACGGUGACCGUCAAtt	s715	s716	s717	**+0.32**	0.06
MYOF	NM_133337	C2 x5	CGAACAACUCUGUAUCGUUtt	GGGACAUCGUUAUCGAAAUtt	GGUUGGACAUGAUUCCGGAtt	s25476	s25477	s25478	**+0.02**	0.03
NBEA	NM_015678	PH-Beach	GGAGACGAUUUGUUCGCAAtt	GGAUGUGAAAGCGAUAGUAtt	CGGACUACAAUGUUUCGUAtt	s25649	s25650	s25651	**+0.02**	0.08
NBEAL1	XM_001134432	PH-Beach	GGAUAUAACAGCUAGAGUAtt	CUAGUGCCUUGAGAGAUAAtt	CUAUGGUACUCACUAUUCAtt	s35186	s35187	s35188	**+0.00**	0.02
NBEAL2	XM_941211	PH-Beach	CCAUUGACAAGUUCCACUAtt	GCUACUUCCAUGUCCUUAAtt	CCAUACUGCUGUUACGUCUtt	s23313	s23314	s23315	**-0.25**	0.03
NCF1	NM_000265	PX	CGAGUUCCAUAAAACCUUAtt	AGGGCACACUUACCGAGUAtt	AGACAUACUUGAUGCCCAAtt	s57647	s57648	s57649	**+0.45**	0.12
NCF4	NM_000631	PX	AAGUCUACGUGGGUGUGAAtt	GGAGGAUCCAAGUACCUCAtt	CCUCAGUCGGAUCAACAAAtt	s9306	s9307	s9308	**+0.49**	0.18
NEDD4L	NM_015277	C2	CAGAUAACCCUGAAUGACAtt	GGACAUCGCGAGUACCUAUtt	CCUUUGAAGAUUUACGAGAtt	s23569	s23570	s23571	**-0.15**	0.04
NISCH	NM_007184	PX	GCCCAUCCUCUCUAACCAAtt	GAAUCAUGUUCGUUCAGGAtt	GGAUCGAACAGAUGGAGGAtt	s22092	s22093	s22094	**+0.45**	0.08
NOXO1	NM_144603	PX	CAAGAGGCUCCAAACGUUUtt	UGCGCGUGUUGGAAACGUCtt	GGAGUUGGGACGAAUUCAGtt	s195651	s195652	s195653	**+0.90**	0.20
NSMAF	NM_003580	PH-Beach, GRAM	CAACGGAUUUUAAAGAGUUtt	GGUGUAGACUUGAACAGCAtt	GCAAGCACACUGUUAGUUUtt	s16015	s16016	s16017	**+0.47**	0.08
OXR1	NM_181354	GRAM	CUAACGAACUUGUUCAAUUtt	GGAUUCUUUGAAUAGCAUAtt	CAAUUGAGGAUUCUAGUAAtt	s30111	s30112	s30113	**+0.05**	0.08
PCLO	XM_940805	C2 x2	CCACUAGUGAAACAACCAAtt	GGAUUACCUGUUACAAGAAtt	GGAGGACUUCAUUCGAAAAtt	s26249	s26250	s26251	**-0.28**	0.04
PDZD8	NM_173791	C1	GCAUAUCCAUAUACAACAAtt	CAAUACUAGUUCUCGUUUAtt	GAGUUCUAUUAAGACGGUUtt	s42265	s42266	s42267	**+0.04**	0.09

PICALM	NM_001008660	ENTH	GGAUAUGACAUGUCUACAUtt	GGCAAGCACUGGUCUAUCUtt	CCACCUAGCAAGUUAGUAUtt	s15799	s15800	s15801	**-0.09**	0.05
PIK3C2A	NM_002645	PX, C2, C2	GCCUACAACUUGAUAAGAAtt	GGAUCUUUUUAAACCUAUUtt	GGCUUUGAGUUGUCAAGCAtt	s10508	s10509	s10510	**-0.04**	0.11
PIK3C2B	NM_002646	PX, C2	GCUCUGAUCCUACCCUUAAtt	CCUACAACCUCAUUCGCAAtt	CGGAAAACCUGCAAUCCUAtt	s10511	s10512	s10513	**-0.02**	0.11
PIK3C2G	NM_004570	PX, C2	CCAUCUACCAGCUAAUCAAtt	GUAGCAUUCCUCCAACAAAtt	GCUACUGGGUGGGAGUAUAtt	s10514	s10515	s10516	**+0.28**	0.14
PIKFYVE	NM_152671	FYVE	CACUGAGGAUGAACGCAAAtt	GGAAAUCUCCUGCUCGAAAtt	CACCGCUACUGGUUGAGAAtt	s47254	s47255	s47256	**+0.23**	0.11
PLA2G4A	NM_024420	C2	GGGCUUGAAUCUCAAUACAtt	GAAUUUAGUCCAUACGAAAtt	CCGUAUCCCUUGAUACUGAtt	s10592	s10593	s10594	**-0.42**	0.03
PLCB3	NM_000932	C2	GCAUAACACCUAUCUCACUtt	CGUCCUUUGUGGAGACCAAtt	GGCUGCUCAUCGAAAAGUAtt	s10619	s10620	s10621	**-0.32**	0.05
PLCD1	NM_006225	PH, C2	CAACAAGAAUAAGAAUUCAtt	GGACCAGCGCAAUACACUAtt	GGAGUUUGCGUUUGAGGUAtt	s10625	s10626	s10627	**+0.60**	0.12
PLCD3	NM_133373	C2	UGGUCAACGUGGACAUGAAtt	GCAGCUCAUUCAGACCUAUtt	GGUUUGUGGUGGAAGAUUAtt	s41418	s41419	s41420	**+0.39**	0.11
PLCG1	NM_182811	PH x2, C2	GGGUGAAAAAGAUCCGUGAtt	GAAUCGUGAGGAUCGUAUAtt	GGACUUUGAUCGCUAUCAAtt	s10631	s10632	s10633	**+0.22**	0.06
PLCG2	NM_002661	PH, C2	GGAUCUCCUCGUCACAUAAtt	CAAUAUGGAAAGAGAUAUAtt	GGGAUUCCAUUGACCAGAAtt	s10634	s10635	s10636	**+0.11**	0.12
PLCH1	NM_014996	PH, C2	GGACGAAUGAUGCAGUUAAtt	CCAGUGUAUUAGUAAGAGUtt	GCAUAGAAGGCUUCACGAAtt	s22817	s22818	s22819	**-0.02**	0.07
PLCL2	NM_015184	PH, C2	GCCGGAGUGUUGAAUUAGAtt	GGACUGCGGUACCUAAUUUtt	CCGUGGAUGAGGUAUUCAAtt	s23334	s23335	s23336	**+1.01**	0.29
PLD1	NM_002662	PX, PH	GCACUAUAUCUAUAUCGAAtt	CACUAUAUCUAUAUCGAAAtt	GGCACUAUAUCUAUAUCGAtt	s10637	s10638	s10639	**-0.15**	0.07
PLD2	NM_002663	PX, PH	CCAUGUCUUUCUAUCGCAAtt	GUGUGAUUCUUGGAGCAAAtt	GAAGAAAUACCGUCAUUUUtt	s10640	s10641	s10642	**-0.01**	0.09
PLEKHF1	NM_024310	FYVE, PH	CACAGGUCUUGGUAACAAAtt	CCAGCUGUCUCAUGCCUUUtt	CCUUUUUGCUGGACACUGUtt	s35643	s35644	s35645	**-0.07**	0.09
PLEKHF2	NM_024613	FYVE, PH	CUAAAUCUUUUGCAGUUUAtt	GUAUAAGUAUAGUGGAAAAtt	GGAGAAGGAGUAUUGACUAtt	s36049	s36050	s36051	**+0.23**	0.11
PLEKHM1	NM_014798	PH x2, C1	GCAGAUCGGCUUCUCCUUUtt	GCACCUCAUUGGGAGGAGAtt	GGAUCAUCCACAACUGGGAtt	s19041	s19042	s19043	**+0.07**	0.12
PRKCA	NM_002737	C2, C1 x2	CAACGUACCCAUUCCGGAAtt	GGCUGUACUUCGUCAUGGAtt	GCUCCACACUAAAUCCGCAtt	s11092	s11094	s11093	**+0.23**	0.04
PRKCB	NM_212535	C2, C1 x2	GGUCUGUUCUUCUUACAGAtt	GGAUGAAACUGACCGAUUUtt	GAAUCGGACAAAGACAGAAtt	s11095	s11096	s11097	**+0.30**	0.10
PRKCD	NM_212539	C2, C1 x2	GGGACACUAUAUUCCAGAAtt	GGAUUAAAGUGUGAAGACUtt	GGAGUGACCGGAAACAUCAtt	s11099	s11098	s11100	**-0.57**	0.04
PRKCI	NM_002740	C1	GAGACCUAAUGUUUCAUAUtt	GGAUAUGAUGGAGCAAAAAtt	GUAAUUCCAUAUAAUCCUUtt	s11110	s11111	s11112	**-0.24**	0.07
PRKCZ	NM_002744	C1	CGUUCGACAUCAUCACCGAtt	GGACUUUGACCUAAUCAGAtt	CGAGGAUAUUGACUGGGUAtt	s11128	s11129	s11130	**+0.42**	0.08
PRKD2	NM_016457	PH, C1 x2	CAGUGGGCGUGAUCAUGUAtt	GAACAACACGACCAACAGAtt	AGAUGAUCCUGUCCAGUGAtt	s24644	s24645	s24646	**-0.08**	0.10
PTEN	NM_000314	C2-tensin type	GCAUACGAUUUUAAGCGGAtt	CACCGCAUAUUAAAACGUAtt	GGUUUUCGAGUCCUAAUUAtt	s325	s326	s327	**+0.18**	0.10
PXK	NM_017771	PX	CGGAAUAUAUUAUUCGAGUtt	GGAUCUGAUCUACAAGGCAtt	GACAUAGGUUGGAGAAUAAtt	s29710	s29711	s29712	**+0.24**	0.08
RAB11FIP1	NM_001002814	C2	ACGAUGAGCUGAUUCAGCUtt	CGAGCUGGAAGACUACAUUtt	AGAAGGAAACGAUAAGCAAtt	s37090	s37091	s37092	**+0.89**	0.09
RAB11FIP2	NM_014904	C2	GCGCAUUCAAUGUCUGAUUtt	GGUUUAGAUUAGAAUCCAAtt	CGAGCUACCUGGAUUGCUAtt	s22475	s22476	s22477	**+0.56**	0.02
RAB11FIP5	NM_015470	C2	GGAACGCGGCGAGAUUGAAtt	GAAGAAGUAUGAUCUGGAAtt	GGCCGCGAGAAGUACAGUAtt	s25026	s25027	s25028	**+0.05**	0.08

RACGAP1	NM_013277	C1	CAGUGACUGUUCCCAAUGAtt	CAACUAAGCGAGGAGCAAAtt	GCGAAAAGCUGGAACGACAtt	s26550	s26551	s26552	**+0.67**	0.09
RAF1	NM_002880	C1	GGAACUGUUUAUAAGGGUAtt	GGAUUUCGAUGUCAGACUUtt	CGUGUUUUCUUGCCGAACAtt	s11749	s11750	s11751	**+0.91**	0.06
RASA1	NM_002890	PH, C2	CAUAGAUCACUAUCGAAAAtt	GAAUCGUUGUUGUUAUGCAtt	CCACGGAUGUUCAAUAUCAtt	s11820	s11819	s11821	**-0.28**	0.07
RASA3	NM_007368	PH, C2 x2	CUCUUCAACUUGUACAUGAtt	GAAUUUACCUACCACAAAAtt	GCCCAUCGUGCUUAAAGAAtt	s355	s357	s356	**+0.37**	0.12
RASAL2	NM_170692	PH, C2 x2	GGAUCAUGCUGAGAUGCAAtt	GCAGGACAGUUCAACCUAAtt	CUAGUGAACUGAUAGACCAtt	s18125	s18126	s18127	**-0.11**	0.06
Rbsn	NM_030081	FYVE	GAAAGUAUAUGAGCUAAUAtt	GGAUAUGAAUCAUUCAGUUtt	GGAAGAUCGUGAUGUCAAAtt	s95445	s95446	s95447	**+0.41**	0.19
RIMS1	NM_014989	FYVE, C2 x2	GUGCAUCGAUUUAAGCAGAtt	GCAUUCACCAGAACGAGAAtt	GGCUAUAGGUCUAGUGCUAtt	s22808	s22809	s22810	**-0.04**	0.10
RIMS2	NM_014677	FYVE, C2 x2	CUACCGAAGUGAUCCGAAUtt	GCGAAUACCUGAUAGCACAtt	CCAACACGGAGGUUGCAAAtt	s18683	s18684	s18685	**+0.35**	0.10
ROCK1	NM_005406	PH, C1	GGUUAGAACAAGAGGUAAAtt	CGGUUAGAACAAGAGGUAAtt	GCUUGUAGGUGAUACACCUtt	s12097	s12098	s12099	**-0.19**	0.06
ROCK2	NM_004850	PH, C1	GGAGAUUACCUUACGGAAAtt	GAGAUUACCUUACGGAAAAtt	GGAUCGAACCCAUGGAUCAtt	s18161	s18162	s18163	**+0.34**	0.10
RPH3A	NM_014954	FYVE, C2 x2	GAGUUUUUCUAUGACAUCAtt	CGAAUUCAAUGAGGAGUUUtt	CCUUGAAUCCCGAAUUCAAtt	s22610	s22611	s22612	**+0.01**	0.10
RPH3AL	NM_006987	FYVE	GCUCGUCGGUGUUCUGCAAtt	GGACCGGAAAGGCGACAAAtt	GAUAGUGACUCGGAUCUUAtt	s18218	s18219	s18220	**+0.03**	0.09
RPS6KC1	NM_012424	PX	GGAAUGGUGUUGAUACAAAtt	GGCAAACUGUGGUCAUAUAtt	CAAAUCCUAUAGUAUAACAtt	s25624	s25625	s25626	**+0.19**	0.06
RUFY1	NM_001040451	FYVE	CGACUAGUGUCAGAAAUCUtt	GGAAAAACCAACCAAGUUAtt	GAAUUACUGAUGUCCUUGAtt	s37102	s37103	s37104	**+0.07**	0.08
RUFY2	NM_017987	FYVE	GAGCUAGCAGUACAAGUUAtt	GGAUGUAGAGAAUGAGCUAtt	GAUUGAAGAGUUAGCAAUAtt	s31236	s31237	s31238	**+0.27**	0.12
RUFY4	NM_198483	FYVE	GCAACAAAGGAAGACUCUAtt	AGAAGAUCCCAGCCGCAUAtt	GAAAGUUCCAGGAAACAUAtt	s49837	s49838	s49839	**-0.13**	0.09
SBF1	NM_002972	PH, GRAM	CUAAGACUGUGGACGAGAAtt	ACACGGAGGUGUUCAGGAAtt	GCACUGCUGUUUCCUCUCAtt	s12482	s12483	s12484	**+0.57**	0.07
SBF2	NM_030962	PH, GRAM	GAUGAUGAAUUGUACUCUAtt	GCACUAUUAAAAUUCCCGAtt	GGACUGGGAUGAUACACCUtt	s37818	s37819	s37820	**+0.36**	0.08
SGK3	NM_001033578	PX	GAGCAUUCCUUCAAAUGGAtt	GAGCAGGACUAAACGAAUUtt	CAUUAUUCCUUCCAAACAAtt	s24316	s24317	s24318	**+0.03**	0.05
SH3PXD2A	NM_014631	PX	GCUGGUGGUAUAUCAGAUAtt	GAAGGCUGGUGGUAUAUCAtt	CCAUGAUCCUGGAACAGUAtt	s18542	s18543	s18544	**+0.32**	0.11
SH3PXD2B	NM_001017995	PX	AGGUCGAGGUGAUCGAGAAtt	GCACAUUGGGAAAAAGAAAtt	CCAUGGAAGGAGGACAGAAtt	s49972	s49973	s49974	**+0.22**	0.12
Non-target control			AGUACUGCUUACGAUACGGtt	UAACGACGCGACGACGUAAtt	UCGUAAGUAAGCGCAACCCtt	s229084	s813	s814	**+0.04**	0.05
SMURF1	NM_020429	C2	CCUGCCCAGAGAUACGAAAtt	GCAUGAACUGAAACCCAAUtt	CCAUAUGAGUCCUAUGAGAtt	s32796	s32797	s32798	**+0.34**	0.06
SMURF2	NM_022739	C2	CACACUUGCUUCAAUCGAAtt	CACUUGCUUCAAUCGAAUAtt	CCGGAACAUUUAUCCUAUUtt	s34857	s34858	s34859	**-0.38**	0.07
SNAP91	NM_014841	ENTH	GGAAUUUCUGGUACCACAAtt	CAAACGAUUUCUAACUAGAtt	GUUAUUAACUUACUCGAAAtt	s19161	s19162	s19163	**+0.10**	0.06
SNX1	NM_003099	PX	GGGCCGCUUUAGAAAGGUAtt	GCCUCAUAGGGAUGACAAAtt	CAACAGUGGUCCGAAAAGAtt	s13255	s13256	s13257	**+0.26**	0.07
SNX10	NM_013322	PX	GGCAGAGACUCCAAAGUAAtt	GAUAUGUAUUCAUACUAAUtt	GCACUUUUGCUUUCAGAUAtt	s26643	s26644	s26645	**+0.55**	0.08
SNX11	NM_152244	PX	CUCCAGUUGUUGACUCUGAtt	CCUCCAUACCAACAGCAAAtt	AGAUAUUCCUCCAUACCAAtt	s26697	s26698	s26699	**-0.05**	0.06

SNX12	NM_013346	PX	UGAGGAGUCUUUCAUCGAAtt	CCACCUAUGAGGUUCGCAUtt	CUACCUAUCUUCAAGCUAAtt	s26739	s26740	s26741	**+0.14**	0.12
SNX13	NM_015132	PX	GGAUGAAGUAUUCGACUUAtt	GAGUAGCAGGAAAAACGAAtt	CGGCUCAACUUGACGAUAAtt	s23163	s23164	s23165	**-0.07**	0.06
SNX14	NM_020468	PX	GAAAUUUGCAGAACCUAGAtt	CGUUUGGUCUCACUCAUAAtt	GAACAUUGGUCUGUCUAUAtt	s32927	s32928	s32929	**+0.01**	0.06
SNX15	NM_013306	PX	CCGCGCAGUUCAUCUCAAAtt	AGGAAGGUGUGAAGAAGAAtt	UCGCUUCACUGUGCACAUAtt	s26682	s26683	s26684	**+0.43**	0.14
SNX16	NM_022133	PX	GGGUCCAUUUGAUAGCCUAtt	GAUAGACCAUCUACACCUAtt	CACUUGAGGUUGAUCAAGAtt	s34409	s34410	s34411	**+0.34**	0.07
SNX17	NM_014748	PX	GCUUUAUGCUCAGACGGUAtt	GGGAGUCUAUGGUCAAACUtt	GUCUAUUCUUAGUUCGAGAtt	s18903	s18904	s18905	**-0.03**	0.06
SNX18	NM_052870	PX	AGGUGACCGGCUUCAAAAAtt	CAUCAUCCACGUUCAGAAAtt	GCAGCGAUGAUGACUGGGAtt	s41342	s229521	s229522	**+0.15**	0.08
SNX19	NM_014758	PX	CACAUGCAAUGUAAUCUUAtt	CACUGUGAAUCGUCGCUAUtt	GUAUUGCCUUUGUCAAGAAtt	s53225	s53226	s53227	**-0.05**	0.07
SNX2	NM_003100	PX	GCGACUUUCUUGGUUUGCAtt	GAACAGAUAUCUAAAACGAtt	GCAUAUAGAGUAACAACAAtt	s13258	s13259	s13260	**+0.34**	0.10
SNX20	NM_182854	PX	GCAUCGAGGAGAGAAAAGUtt	AGUUUGUGGUGUACCAAAUtt	GCAUGGGACCCAUAACCCAtt	s42740	s42741	s42742	**-0.19**	0.07
SNX21	NM_152897	PX	GAACGAGUCUUGUUUCUCUtt	GCCGUUACUCGGACUUUGAtt	UGGUAAUUCAUGAAAAAUAtt	s40288	s40289	s40290	**+0.04**	0.06
SNX22	NM_024798	PX	GAAUUUGUAUGCUCUUAGAtt	GCUUCCAUGUGGAUCCCUAtt	GGCAGGGUCAAGAAGAUAAtt	s36495	s36496	s36497	**-0.04**	0.08
SNX24	NM_014035	PX	CGACGACAAGGCUUGGAAAtt	GGCAGAAAGUUGUGGAUCUtt	CUUCUAAACAUGUUAGGAAtt	s26312	s26313	s26314	**+0.10**	0.06
SNX25	NM_031953	PX	GUCUCUCAGCUUACGUAUAtt	GGAUGAAAUAAUCCUAAUAtt	GCGAGUUUCAGAAUUUACAtt	s38290	s38291	s38292	**+0.13**	0.06
SNX27	NM_030918	PX	GAACAGUACUACAGACCAAtt	GGAACAACGGUUACAGUCAtt	GCAUUUGAAUGGGAUGAGAtt	s37695	s37696	s37697	**-0.20**	0.06
SNX29	XM_001131890	PX	GAGUUUGUCGGAUUUUGAAtt	GAAUAUUUAUCGCCGGUAUtt	AGACGAUGAAUGGAAUAUUtt	s40838	s40839	s40840	**+0.33**	0.08
SNX3	NM_003795	PX	GCUGCGAAGUGAAUUAGAAtt	GAAUCUACUGUUAGAAGAAtt	AGACAAAUCUUCCUAUUUUtt	s16618	s16619	s16620	**+0.41**	0.11
SNX30	XM_376902	PX	CAGCUUCGGUGACAAGGAUtt	CCAGCCCACUCAUCUCAUUtt	GGGAACCAUUGAUCGAAUAtt	s53639	s53640	s53641	**-0.12**	0.08
SNX31	NM_152628	PX	GCAGAUUGAAGUUCCGGAAtt	GAACUCUGCUGGAUACGGAtt	CCAUGGACCCAAACGUGUUtt	s46737	s46738	s46739	**-0.20**	0.10
SNX32	NM_152760	PX	GCACCCUGAUUCUCCGGAAtt	AGGUGAAAUUCACUGUUCAtt	GAAAUUCACUGUUCAAACAtt	s48495	s48496	s48497	**-0.02**	0.07
SNX33	NM_153271	PX	CAACCGUUUCUCAUGCUUUtt	CAAAUUCAAGGGCAUCAAAtt	GGCCGUAACCUCAACCGUUtt	s48887	s48888	s48889	**+0.17**	0.10
SNX4	NM_003794	PX	CAAGCUCUUUGGUCAAGAAtt	GCGACGGAUUGGUUUAGAAtt	GCUACCUUUUAGUUUACUAtt	s16615	s16616	s16617	**-0.01**	0.07
SNX5	NM_152227	PX	GAGUUAAGGAGGUAGAUGAtt	CUGUAUCUGUGGACCUGAAtt	CGAUACUACAUGCUCAACAtt	s25876	s25877	s25878	**+0.26**	0.07
SNX6	NM_152233	PX	GGUCACUAGUGGAUUAUGAtt	GCAGAUGGAGUAAUCGUUUtt	GGAGAAGGGUCAAUGACGAtt	s33937	s33938	s33939	**-0.22**	0.07
SNX7	NM_015976	PX	CAAUGAUAAACCAAAUCAAtt	GAAACUUUCAUUACGUAUAtt	CCGAAUUGCUGAUCAUCCAtt	s28045	s28046	s28047	**+0.54**	0.15
SNX8	NM_013321	PX	CAAUAGCUUUCACAAGCUUtt	GAUCUUCUCAUAUUCGGGAtt	CGUCAACUCUCAGAUCCAAtt	s26640	s26641	s26642	**+0.09**	0.09
SNX9	NM_016224	PX	CAGUCGUGCUAGUUCCUCAtt	GCAUCAUGUCUUACGCGUUtt	GCAGUUCCUAAAUUUCCGAtt	s28123	s28124	s28125	**-0.10**	0.06
SYNGAP1	NM_006772	PH, C2	CGAACGAAGUCACAACCCAtt	GCACCGAACCCAAUACGUUtt	GCACGUUACCAGACAAUGAtt	s16846	s16847	s16848	**+0.83**	0.20
SYT7	NM_004200	C2 x2	CCAUCAUCGUGAACAUCAUtt	UCCAAGUCCUGGACUAUGAtt	AGAAGACGGUGACGAUGAAtt	s17291	s17292	s17293	**-0.05**	0.11

SYTL1	NM_032872	C2 x2	CCUGGGUCGCAACAUCUUUtt	GAAGGACUGUUGGACCUCAtt	ACAUCUUUCUGGGCGAAGUtt	s39754	s39755	s39756	**+0.77**	0.09
SYTL2	NM_032379	C2 x2	GGACUCUACUUCAGAGGAAtt	GGGAUACAUUUAAGCGCAAtt	GGACUGAAGUGGACUGGAUtt	s29567	s29568	s29569	**+0.95**	0.08
SYTL4	NM_080737	C2 x2, FYVE-type	GCGGGACACUAUUAAUCCAtt	GAGUUACUGGAGAUAAAAAtt	GGAAAUAGAGUUGAAGAAAtt	s230068	s230069	s230070	**-0.05**	0.10
SYTL5	NM_138780	C2 x2, FYVE-type	GGUUUGUGCUUCAACCCAAtt	CUCUUAGAAGCAAAACGUAtt	CAACAAGCGUAAGACCAAAtt	s41275	s41276	s41277	**-0.26**	0.09
TBC1D8	NM_001102426	GRAM x2	GAACGAAACGGGAAUUGCUtt	CUCUACGACUUAUUCAAGAtt	CUAUUAUACAGGCUUCAUAtt	s230654	s230655	s230656	**+0.34**	0.05
TBC1D8B	NM_198881	GRAM x2	GGACUCUACUGCUAAAGUAtt	CUACUAAUCCUGACUAUUAtt	GGCAAUCAGUGUAGUGUAAtt	s29674	s29675	s29676	**+0.02**	0.06
TBC1D9	NM_015130	GRAM x2	GCGAUGAUGUGGAACCUUAtt	CUAUUACUCUUGCAGCUAUtt	GGAUUUGAACAAGAUCGAUtt	s23160	s23161	s23162	**+0.23**	0.06
TBC1D9B	NM_198868	GRAM x2	CGUGAUUUCUUGGUGCAGAtt	CAGAUGCGGUUUAAACAGAtt	GAGUGGACAUUGGACUCAAtt	s22941	s22942	s22943	**+0.14**	0.05
TNS1	NM_022648	C2-tensin type	GUUCCGCUCUCAAUCCUUUtt	CCAGGACACUUCUAAGUAUtt	CCAUCAUGCAGCAGAAUAAtt	s14299	s14300	s14301	**+0.24**	0.12
Tns2	NM_153533	C1, C2-tensin type	CCUGAGCUGUUGACAAGCAtt	CCCAUGUGCUUCAAUCCAAtt	GAACACCCUUUACAAGAGAtt	s102008	s102009	s102010	**-0.09**	0.04
TNS3	NM_022748	C2-tensin type	GCUCAUUCAUUGUUCGAGAtt	CUUACGAAGCUUAACCCAAtt	GGAUCUGCAUCGUCAUCGAtt	s34875	s34876	s34877	**+0.24**	0.11
TPTE	NM_199261	C2-tensin type	CGUUAUGUACGUGAUCUAAtt	GAAAAUGUUCGGUACUUGAtt	AGAAGAGAUAUGUUGCAUAtt	s14361	s14362	s14363	**+0.73**	0.11
ULK1	XM_001133335	None	GCAUCGGCACCAUCGUCUAtt	GCAUCGGCACCAUCGUCUAtt	GCAUCGGCACCAUCGUCUAtt	s15963	s15963	s15963	**-0.93**	0.02
UNC13A	NM_001080421	C2 x3, C1	GGUCCAAGCUGAUUACCCUtt	GCAUCACCUUCUUUCGGAUtt	CAAUGAGUAUGUGACGGAAtt	s22857	s22858	s22859	**+0.07**	0.09
UNC13B	NM_006377	C2 x3, C1	GAAGCGUACCAAGACCAUUtt	GGAUUGCGCUGAAGACUAUtt	GCACUUCUCUUAAGGACGAtt	s20574	s20575	s20576	**-0.38**	0.02
UNC13D	NM_199242	C2 x2	ACUGAAUGGUUCCACCUGAtt	GGGACAAGAUCUUCCACAAtt	GAGCUUUGCUACAUGAACAtt	s47356	s47357	s47358	**-0.52**	0.07
VAV2	NM_003371	PH, C1	CGUUUGACAAGACCACCAAtt	GCCUGCAAAAUGUUCCUCAtt	CAGCAUCGCGCAGAACAAAtt	s14753	s14754	s14755	**+0.73**	0.08
VPS36	NM_016075	GLUE	CAGUUACCAGAGAAACCUAtt	GCCCAUUCCAGAGUAGUAAtt	CCCAGUCAUUACAAACAAAtt	s27276	s27277	s27278	**+0.41**	0.08
WBP2	NM_012478	GRAM	CCGUAUUUGGUGCAAACUAtt	AGAGCAUCCUAAUGUCCUAtt	GCAUCCUAAUGUCCUAUGAtt	s24092	s24093	s24094	**+0.76**	0.04
WBP2NL	NM_152613	GRAM	GCCCGAGGAUUUCCACUUAtt	CUUCAUUAAGGGAACUAUUtt	UCAGCUCUAUGGGAAUUUAtt	s46539	s46540	s46541	**-0.45**	0.04
WDFY1	NM_020830	FYVE	GGGUGUCUGCGAUUAUCUUtt	GCUCCUCAGUGGUUGGAAAtt	AGAUGAAGAUCGGACUUCUtt	s33388	s33389	s33390	**-0.02**	0.08
WDFY2	NM_052950	FYVE	GCAUGUCUUUUAACCCGGAtt	GGAACUGACAAGGUUAUUAtt	GACUGUCCAUAGGUCUAGAtt	s41881	s41882	s41883	**+0.03**	0.04
WDFY3	NM_014991	FYVE, PH-Beac	GCUUAAAUUAUAUACCUUGtt	UGGUUAAUCUGAUAACUUCtt	GCACAUGACUCAGAAGGAAtt	s200499	s200500	s200501	**+0.19**	0.07
WDFY4	NM_020945	PH-Beach	GGAAGACUGAGGAUGUGAAtt	GACAAGUUAUUUUACAAGAtt	GGUUUAAAGAAGUUGAGAAtt	s229872	s229873	s229874	**+0.24**	0.06
WDR45	NM_007075	PROPPIN	UCCCAGAAGGGUACCCUUAtt	AGAUCGUGAUCGUGCUGAAtt	CGCUUCCAGUGAUAAGGGUtt	s21995	s21996	s21997	**-0.47**	0.04
WDR45B	NM_019613	PROPPIN	GCUGCAACUAUUUAGCUUUtt	CUAUAACACUGAUCCACUAtt	GGAAUAAACAGUCCAGUUUtt	s32117	s32118	s32119	**-0.16**	0.07
WIPI1	NM_017983	PROPPIN	GCACUAUUGCUGCCCAUGAtt	GAAACUCCCUGAAAACAGUtt	CCCUCUCAACGAUCCAGAAtt	s30081	s30082	s30083	**+0.46**	0.07

WIPI2	NM_016003	PROPPIN	GCAGGUCUUCGAUACCAUUtt	GUCUGGAAACGACCAAUGAtt	UGACGCAAGUGGAACUAAAtt	s25100	s25101	s25102	**+0.07**	0.03
WWP1	NM_007013	C2	CAGUAGUUCUUCUAAUCCAtt	GGUUCGGAACAGCAAUAUAtt	GCACGAAUGGAAUAGAUAAtt	s21788	s21789	s21790	**+0.52**	0.05
ZFYVE1	NM_178441	FYVE x2	GGAUGGGUCUCGCAAAAUAtt	GGAUGUAAGAAAAGCAUGAtt	CACUAGGUCUGGUAAAGGAtt	s28712	s28713	s28714	**-0.08**	0.11
ZFYVE16	NM_014733	FYVE	GGUGGAUCUAGUUUCGUAAtt	GCGGCUAGCUUUACGAGAAtt	CCUUCGAAAUUACCAGUAUtt	s18852	s18853	s18854	**+0.41**	0.13
ZFYVE19	NM_001077268	FYVE	GGAGUACGGCUGUAAGAAUtt	AGUUCACCCUCUUCAAGAAtt	CCUUUGAGCUUAAAGAGCAtt	s39700	s39701	s39702	**+0.02**	0.07
ZFYVE21	NM_024071	FYVE, PH-like	GGACAAGGAGUGUCGGAGAtt	CUAUGAAAUCGAAAUUGUAtt	GACUUGUCGUCUUUCCAAUtt	s35465	s35466	s35467	**+0.34**	0.11
ZFYVE26	NM_015346	FYVE	GAAUGGUGUUUUACUCUAUtt	CCUUGCAAGAUGACGAUUAtt	GGAUGUGGUUGAGUACCUAtt	s23943	s23944	s23945	**+0.48**	0.10
ZFYVE27	NM_001002262	FYVE	CAGGUGAUGGUGUUCGAUAtt	CAGCAGAGGAUGAACCCAAtt	GAGCUGCAGUAAUUGUGGAtt	s42248	s42249	s42250	**+0.00**	0.07
ZFYVE28	NM_020972	FYVE	CUCUGAACUUGGACCGCAAtt	GAGAAGUAUUCUUAAAACAtt	GCAUUUCCCAAGACGUGGAtt	s33699	s33700	s33701	**-0.06**	0.07
ZFYVE9	NM_004799	FYVE	GGACUGUAAUCUAAAUCCAtt	CGAUUACAAGUUUAACGGUtt	GGACAUUACAAAACGAUUUtt	s17931	s17932	s17933	**-0.03**	0.07

Oligonucleotide Primers/Probes

Appendix 2 – Oligonucleotide primers/probes

Target	Usage	Forward (5' -> 3')	Reverse (5' -> 3')
AKAP13	qPCR	GCAGAGCCCAGAATGTGAGA	CCATGTCATCACTGGGTGAGT
ARHGEF2	qPCR	TTCTCAGGTCCTAGTGCGGA	CGGGTCACTTTCCGGATGAA
β-actin	ZF, qPCR	CGAACGACCAACCTAAACCTCTCG	ATGCGCCATACAGAGCAGAAGC
BNIP3	qPCR	GGCCATCGGATTGGGGATCT	GGCCACCCCAGGATCTAACA
BNIP3L	qPCR	TCCACCCAAGGAGTTCCACT	GTGTGCTCAGTCGCTTTCCA
CHN1	qPCR	CTAAAGAGAGTGACCCTCCACG	GGGTGGGTCCAAAGACGATT
CPNE2	qPCR	GTGTGCTCAGTCGCTTTCCA	AGGATGAAGTACTGCGTGGC
CPNE7	qPCR	AGGATGAAGTACTGCGTGGC	AGGCCTCTGTGGCTGTAGTA
GAK	qPCR	GTGGAGGAAGAGATCACGAGG	AGATATCCTGCTTCTCGCCG
GRAMD1C	qPCR	GCAACTGCTCCAGCAGAACTA	CTTCTTCCTGGACTTCTTGGCT
HIF1α	qPCR	CTTCTTCCTGGACTTCTTGGCT	GCAGGGTCAGCACTACTTCG
HS1BP3	qPCR	Qiagen – QT00094899	
ITSN1	qPCR	CGGAGATGAGGCGTCGATTA	ACTGCTGATCATGCTTCGCT
ITSN2	qPCR	GGCTCAGTTTCCCACAGCTA	ACGTGCTTGATCACCTGTTATGT
LYST	qPCR	Qiagen – QT00094906	
PRKCD	qPCR	GCAGGGTCAGCACTACTTCG	GCAGGGTCAGCACTACTTCG
prkcda	ZF, qPCR	TTGGCGTATCTGTGTTGGCT	ATGACGACACACTGAGCCTG
prkcdb	ZF, qPCR	ACAAAAATGTGCCAGCGGAC	ACGCGAACTGTGGAGACAAT
prkcda	5'UTR ISH Probe	GCTCTGCCTGAGGGGTTGCCATGGC	GAGGCCTTGTTTGACAAGACCC
prkcda	ORF ISH Probe	CTGCTGGCAGAAGCTCTTACTCAAG	GAAGGTTGTGGCCCGATTGTCTCC
prkcda	sgRNA #1 (Exon 2)	taatacgactcactataGGGGCCATGGCAACCCCTCgttttagagctagaa	
prkcda	sgRNA #2 (Exon 11)	taatacgactcactataGGGTGGGTGATTCGAGATGGgttttagagctagaa	
prkcda	sgRNA #3 (Exon 15)	taatacgactcactataGGGAGTTCCGCAGAAGGTTGgttttagagctagaa	
prkcdb	5'UTR ISH Probe	GAAGCTGTGATCTCTCACCATG	CCGCAGAGGTTGGCAACCTTTG
prkcdb	ORF ISH Probe	CGGAGGGCTCTCAGTATGGG	GGACGTCCATGCGGATGGAG
prkcdb	sgRNA #1 (Exon 2)	taatacgactcactataGGTCACCATGGCTCCGTTCCTGgttttagagctagaa	
prkcdb	sgRNA #2 (Exon 8)	taatacgactcactataGGTAGCCTGGTACGCGGTTTgttttagagctagaa	
prkcdb	sgRNA #3 (Exon 14)	taatacgactcactataGGGCCTCTTTGGTGATCCAGgttttagagctagaa	
RAB11FIP1	qPCR	GCAGGGTCAGCACTACTTCG	GCAGGGTCAGCACTACTTCG
SMURF1	qPCR	TACCGGATACCAGCGTTTGG	ACCACTATCTGGCCACGAAC
SMURF2	qPCR	CATGTCTAACCCCGGAGGC	CAAATGGATCAGGAAGTCGGAAAA
SYTL2	qPCR	CTGTCCATTTGGCATCGGGA	GTGCTGTCTTCCGCTTCAGA
SYTL4	qPCR	ATGTGCCTGGAACTGACTGT	ACTGATCCCAGTGCCAACAC
SYTL5	qPCR	GTGACAAAATCGCGCAGCTA	GGACAACATCAGTGCCGAGA
SNX10	qPCR	CAGAAAGTTCATCCTCTGGGCT	CAGAAAGTTCATCCTCTGGGCT
SNX15	qPCR	GATGACTTCCTGCGGCACTA	ACCACCACCTCTTTGACATCC
TBP	qPCR	CAGAAAGTTCATCCTCTGGGCT	TATATTCGGCGTTTCGGGCA

UNC13B	qPCR	CTCTGCGTGCGCGTTAAAAG	GGAAGGCTGATCACCACGAA
UNC13D	qPCR	CTCAAGGCAGAACAGCAGGA	GAAGACAGAGCGGAACCTCC
WIPI1	qPCR	CCATAAGGCTGAACCGGCA	CATAGACCTGTTGGGTTTGCAG
WIPI2	qPCR	TGCTCGCTAGCCACAATTCA	TGCTTCATCAGGGCACACTC
WDR45B	qPCR	GCCGAAATACCCTCCCAACA	CCACAATTCTATCTCGCCGC
WDR45	qPCR	TCTGTCATTGCCATCTGCGT	CACGTCGAAAGCCTCTCTGT
zFYVE21	qPCR	GTCATGTCCTCCGAGGTGTC	CATCTCCGACACTCCTTGTCC
zFYVE26	qPCR	CCTCAGAGGGAGAAACGATCAG	TACTGGAGATACCAGGAGGAGC

REFERENCES

1. Evans, C. S. & Holzbaur, E. L. F. Quality Control in Neurons: Mitophagy and Other Selective Autophagy Mechanisms. *J. Mol. Biol.* **432**, 240–260 (2020).

2. Montava-Garriga, L. & Ganley, I. G. Outstanding Questions in Mitophagy: What We Do and Do Not Know. *J. Mol. Biol.* (2019). doi:10.1016/j.jmb.2019.06.032

3. Wang, X. Le *et al.* Parkin, an E3 Ubiquitin Ligase, Plays an Essential Role in Mitochondrial Quality Control in Parkinson's Disease. *Cell. Mol. Neurobiol.* (2020). doi:10.1007/s10571-020-00914-2

4. McWilliams, T. G. *et al.* Basal Mitophagy Occurs Independently of PINK1 in Mouse Tissues of High Metabolic Demand. *Cell Metab.* **27**, 439-449.e5 (2018).

5. Lee, J. J. *et al.* Basal mitophagy is widespread in Drosophila but minimally affected by loss of Pink1 or parkin. *J. Cell Biol.* **217**, 1613–1622 (2018).

6. Bruick, R. K. Expression of the gene encoding the proapoptotic Nip3 protein is induced by hypoxia. *Proc. Natl. Acad. Sci. U. S. A.* **97**, 9082–7 (2000).

7. Jaakkola, P. *et al.* Targeting of HIF-α to the von Hippel-Lindau ubiquitylation complex by O2-regulated prolyl hydroxylation. *Science (80-.).* **292**, 468–472 (2001).

8. Allen, G. F. G., Toth, R., James, J. & Ganley, I. G. Loss of iron triggers PINK1/Parkin-independent mitophagy. *EMBO Rep.* **14**, 1127–35 (2013).

9. Zhao, J.-F., Rodger, C. E., Allen, G. F. G., Weidlich, S. & Ganley, I. G. HIF1α-dependent mitophagy facilitates cardiomyoblast differentiation. **4**, 99–113 (2020).

10. de la Ballina, L. R., Munson, M. J. & Simonsen, A. Lipids and lipid-binding proteins in

selective autophagy. *J. Mol. Biol.* (2019). doi:10.1016/j.jmb.2019.05.051

11. Princely Abudu, Y. *et al.* NIPSNAP1 and NIPSNAP2 Act as 'Eat Me' Signals for Mitophagy. *Dev. Cell* **49**, 509-525.e12 (2019).

12. Tang, M. Y. *et al.* Structure-guided mutagenesis reveals a hierarchical mechanism of Parkin activation. *Nat. Commun.* **8**, (2017).

13. Yoshimori, T., Yamamoto, A., Moriyama, Y., Futai, M. & Tashiro, Y. Bafilomycin A1, a specific inhibitor of vacuolar-type H(+)-ATPase, inhibits acidification and protein degradation in lysosomes of cultured cells. *J. Biol. Chem.* **266**, 17707–12 (1991).

14. Shepherd, D. & Garland, P. B. The kinetic properties of citrate synthase from rat liver mitochondria. *Biochem. J.* **114**, 597–610 (1969).

15. Kirkwood, K. J., Ahmad, Y., Larance, M. & Lamond, A. I. Characterization of native protein complexes and protein isoform variation using sizefractionation- based quantitative proteomics. *Mol. Cell. Proteomics* **12**, 3851–3873 (2013).

16. Larance, M., Ahmad, Y., Kirkwood, K. J., Ly, T. & Lamond, A. I. Global subcellular characterization of protein degradation using quantitative proteomics. *Mol. Cell. Proteomics* **12**, 638–650 (2013).

17. Nascimbeni, A. C., Codogno, P. & Morel, E. Phosphatidylinositol-3-phosphate in the regulation of autophagy membrane dynamics. *FEBS J.* **284**, 1267–1278 (2017).

18. Holland, P. *et al.* HS1BP3 negatively regulates autophagy by modulation of phosphatidic acid levels. *Nat. Commun.* **7**, (2016).

19. Pankratz, N. *et al.* Genomewide association study for susceptibility genes contributing

to familial Parkinson disease. *Hum. Genet.* **124**, 593–605 (2009).

20. Liu, J., Chen, J., Dai, Q. & Lee, R. M. Phospholipid scramblase 3 is the mitochondrial target of protein kinase C delta-induced apoptosis. *Cancer Res.* **63**, 1153–6 (2003).

21. Pu, S. Y. *et al.* Optimization of Isothiazolo[4,3- b]pyridine-Based Inhibitors of Cyclin G Associated Kinase (GAK) with Broad-Spectrum Antiviral Activity. *J. Med. Chem.* **61**, 6178–6192 (2018).

22. Asquith, C. R. M. *et al.* SGC-GAK-1: A Chemical Probe for Cyclin G Associated Kinase (GAK). *J. Med. Chem.* **62**, 2830–2836 (2019).

23. Zhang, J. & Ney, P. A. Role of BNIP3 and NIX in cell death, autophagy, and mitophagy. *Cell Death Differ.* **16**, 939–46 (2009).

24. Johansen, T. & Lamark, T. Selective Autophagy: ATG8 Family Proteins, LIR Motifs and Cargo Receptors. *J. Mol. Biol.* **432**, 80–103 (2020).

25. Marinković, M., Šprung, M. & Novak, I. Dimerization of mitophagy receptor BNIP3L/NIX is essential for recruitment of autophagic machinery. *Autophagy* (2020). doi:10.1080/15548627.2020.1755120

26. Kinoshita, E., Kinoshita-Kikuta, E., Takiyama, K. & Koike, T. Phosphate-binding tag, a new tool to visualize phosphorylated proteins. *Mol. Cell. Proteomics* **5**, 749–57 (2006).

27. Scaduto, R. C. & Grotyohann, L. W. Measurement of mitochondrial membrane potential using fluorescent rhodamine derivatives. *Biophys. J.* **76**, 469–477 (1999).

28. Matsuda, N. *et al.* PINK1 stabilized by mitochondrial depolarization recruits Parkin to damaged mitochondria and activates latent Parkin for mitophagy. *J. Cell Biol.* **189**,

211–221 (2010).

29. Petherick, K. J. *et al.* Pharmacological inhibition of ULK1 kinase blocks mammalian target of rapamycin (mTOR)-dependent autophagy. *J. Biol. Chem.* **290**, 11376–11383 (2015).

30. Joo, J. H. *et al.* Hsp90-Cdc37 chaperone complex regulates Ulk1- and Atg13-mediated mitophagy. *Mol. Cell* **43**, 572–85 (2011).

31. Stein, S. C., Woods, A., Jones, N. A., Davison, M. D. & Carling, D. The regulation of AMP-activated protein kinase by phosphorylation. *Biochem. J.* **345 Pt 3**, 437–43 (2000).

32. Knapp, S. *et al.* A public-private partnership to unlock the untargeted kinome. *Nat. Chem. Biol.* **9**, 3–6 (2013).

33. Heo, J. M. *et al.* RAB7A phosphorylation by TBK1 promotes mitophagy via the PINK-PARKIN pathway. *Sci. Adv.* **4**, 1–17 (2018).

34. Kashatus, D. F. *et al.* RALA and RALBP1 regulate mitochondrial fission at mitosis. *Nat. Cell Biol.* **13**, 1108–1117 (2011).

35. Linares, J. F., Amanchy, R., Diaz-Meco, M. T. & Moscat, J. Phosphorylation of p62 by cdk1 Controls the Timely Transit of Cells through Mitosis and Tumor Cell Proliferation. *Mol. Cell. Biol.* **31**, 105–117 (2011).

36. Gavet, O. & Pines, J. Progressive Activation of CyclinB1-Cdk1 Coordinates Entry to Mitosis. *Dev. Cell* **18**, 533–543 (2010).

37. Lee, D.-W., Zhao, X., Yim, Y.-I., Eisenberg, E. & Greene, L. E. Essential role of cyclin-G-

associated kinase (Auxilin-2) in developing and mature mice. *Mol. Biol. Cell* **19**, 2766–76 (2008).

38. Greener, T. *et al.* Caenorhabditis elegans auxilin: A J-domain protein essential for clathrin-mediated endocytosis in vivo. *Nat. Cell Biol.* **3**, 215–219 (2001).

39. Kandachar, V., Bai, T. & Chang, H. C. The clathrin-binding motif and the J-domain of Drosophila Auxilin are essential for facilitating Notch ligand endocytosis. *BMC Dev. Biol.* **8**, 1–15 (2008).

40. Park, B. C. *et al.* The clathrin-binding and J-domains of GAK support the uncoating and chaperoning of clathrin by Hsc70 in the brain. *J. Cell Sci.* **128**, 3811–3821 (2015).

41. Wrighton, P. Quantitative intravital imaging reveals in vivo dynamics of physiological-stress induced mitophagy. 1–45 (2020). doi:https://doi.org/10.1101/2020.03.26.010405

42. Grünblatt, E. *et al.* Gene expression profiling of parkinsonian substantia nigra pars compacta; alterations in ubiquitin-proteasome, heat shock protein, iron and oxidative stress regulated proteins, cell adhesion/cellular matrix and vesicle trafficking genes. *J. Neural Transm.* **111**, 1543–73 (2004).

43. Song, L. *et al.* Auxilin Underlies Progressive Locomotor Deficits and Dopaminergic Neuron Loss in a Drosophila Model of Parkinson's Disease. *Cell Rep.* **18**, 1132–1143 (2017).

44. Nguyen, M. & Krainc, D. LRRK2 phosphorylation of auxilin mediates synaptic defects in dopaminergic neurons from patients with Parkinson's disease. *Proc. Natl. Acad. Sci. U. S. A.* **115**, 5576–5581 (2018).

45. Cowell, C. F. *et al.* Mitochondrial diacylglycerol initiates protein-kinase D1-mediated ROS signaling. *J. Cell Sci.* **122**, 919–28 (2009).

46. Zhang, T., Sell, P., Braun, U. & Leitges, M. PKD1 protein is involved in reactive oxygen species-mediated mitochondrial depolarization in cooperation with protein kinase Cδ (PKCδ). *J. Biol. Chem.* **290**, 10472–85 (2015).

47. Caso, S., Maric, D., Arambasic, M., Cotecchia, S. & Diviani, D. AKAP-Lbc mediates protection against doxorubicin-induced cardiomyocyte toxicity. *Biochim. Biophys. Acta - Mol. Cell Res.* **1864**, 2336–2346 (2017).

48. Zhang, P., Verity, M. A. & Reue, K. Lipin-1 regulates autophagy clearance and intersects with statin drug effects in skeletal muscle. *Cell Metab.* **20**, 267–279 (2014).

49. Botta, P. *et al.* Regulating anxiety with extrasynaptic inhibition. *Nat. Neurosci.* **18**, 1493–1500 (2015).

50. Caserta, T. M., Smith, A. N., Gultice, A. D., Reedy, M. A. & Brown, T. L. Q-VD-OPh, a broad spectrum caspase inhibitor with potent antiapoptotic properties. *Apoptosis* **8**, 345–52 (2003).

51. Lazarou, M. *et al.* The ubiquitin kinase PINK1 recruits autophagy receptors to induce mitophagy. *Nature* **524**, 309–314 (2015).

52. Carpenter, A. E. *et al.* CellProfiler: image analysis software for identifying and quantifying cell phenotypes. *Genome Biol.* **7**, R100 (2006).

53. Thisse, C. & Thisse, B. High-resolution in situ hybridization to whole-mount zebrafish embryos. *Nat. Protoc.* **3**, 59–69 (2008).

54. Stark, C. *et al.* BioGRID: a general repository for interaction datasets. *Nucleic Acids Res.* **34**, (2006).

55. Cline, M. S. *et al.* Integration of biological networks and gene expression data using cytoscape. *Nat. Protoc.* **2**, 2366–2382 (2007).

56. Ge, S. X., Jung, D., Jung, D. & Yao, R. ShinyGO: A graphical gene-set enrichment tool for animals and plants. *Bioinformatics* **36**, 2628–2629 (2020).

57. Kremer, J. R., Mastronarde, D. N. & McIntosh, J. R. Computer visualization of three-dimensional image data using IMOD. *J. Struct. Biol.* **116**, 71–76 (1996).

58. Fang, E. F. *et al.* In vitro and in vivo detection of mitophagy in human cells, C. Elegans, and mice. *J. Vis. Exp.* **2017**, 1–9 (2017).

59. Fang, E. F. *et al.* Mitophagy inhibits amyloid-β and tau pathology and reverses cognitive deficits in models of Alzheimer's disease. *Nat. Neurosci.* **22**, 401–412 (2019).

60. Palikaras, K., Lionaki, E. & Tavernarakis, N. Coordination of mitophagy and mitochondrial biogenesis during ageing in C. elegans. *Nature* **521**, 525–528 (2015).

61. Jao, L.-E., Wente, S. R. & Chen, W. Efficient multiplex biallelic zebrafish genome editing using a CRISPR nuclease system. *Proc. Natl. Acad. Sci. U. S. A.* **110**, 13904–9 (2013).

62. Montague, T. G., Cruz, J. M., Gagnon, J. A., Church, G. M. & Valen, E. CHOPCHOP: A CRISPR/Cas9 and TALEN web tool for genome editing. *Nucleic Acids Res.* **42**, 401–407 (2014).

63. Emran, F., Rihel, J. & Dowling, J. E. A behavioral assay to measure responsiveness of

Zebrafish to changes in light intensities. *J. Vis. Exp.* 1–6 (2008). doi:10.3791/923

64. Casado, P. *et al.* Kinase-substrate enrichment analysis provides insights into the heterogeneity of signaling pathway activation in leukemia cells. *Sci. Signal.* **6**, 1–14 (2013).

65. Cox, J. & Mann, M. MaxQuant enables high peptide identification rates, individualized p.p.b.-range mass accuracies and proteome-wide protein quantification. *Nat. Biotechnol.* **26**, 1367–1372 (2008).

66. Tyanova, S. *et al.* The Perseus computational platform for comprehensive analysis of (prote)omics data. *Nat. Methods* **13**, 731–740 (2016).

Figure 1

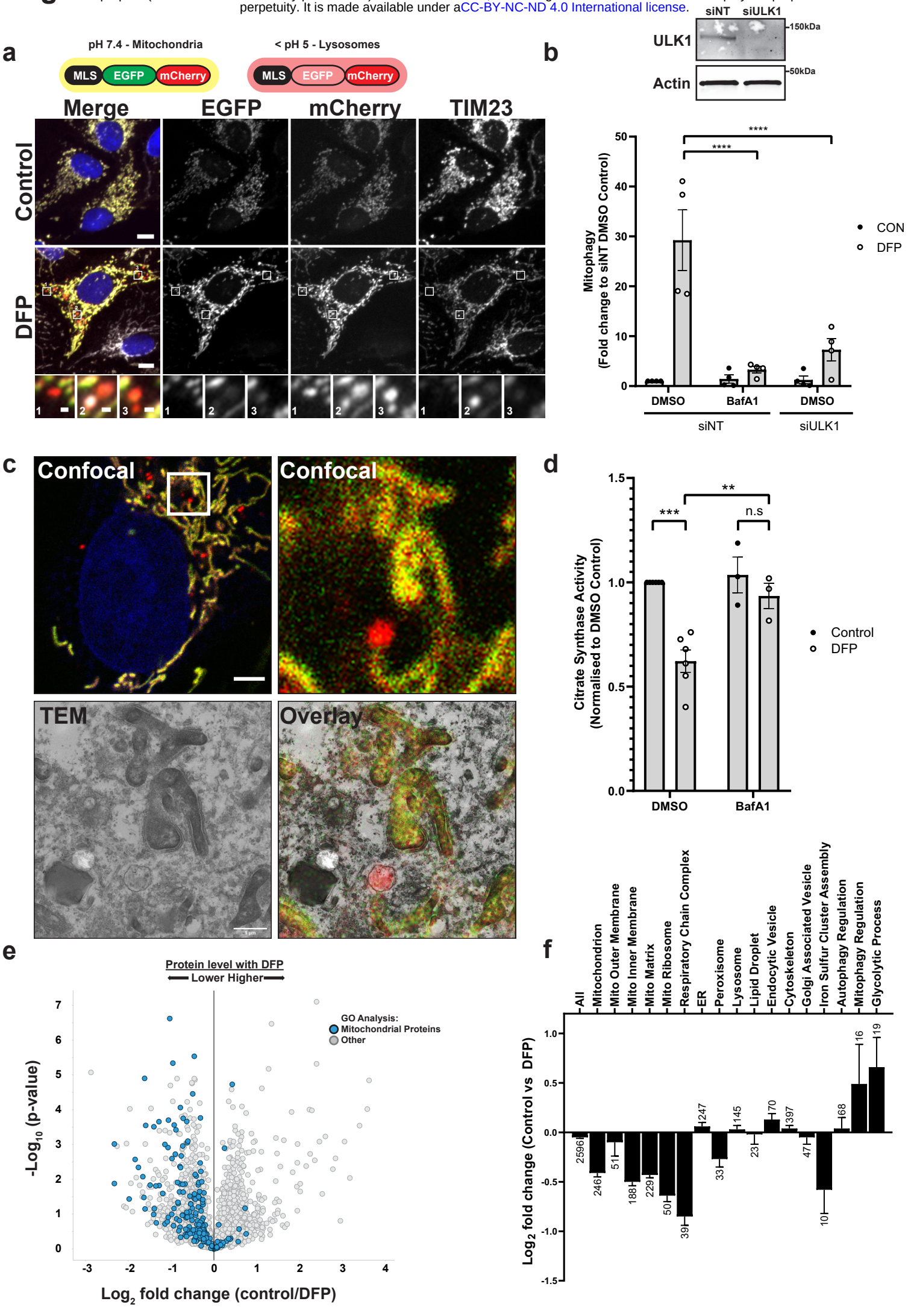

Figure 1 - Measuring DFP-induced mitophagy in vitro

a U2OS cells stably expressing an internal MLS-EGFP-mCherry (IMLS) reporter that is pH responsive (yellow at neutral, red at acidic pH) were incubated for 24 h ± 1mM DFP followed by PFA fixation, antibody staining for TIM23 (Alexa Fluor-647) and widefield microscopy. Scale bar = 10 μm, inset = 0.5 μm. **b** U2OS IMLS cells were transfected with 7.5 nM siRNA non-targeting control (siNT) or siULK1 for 48 h prior to 24 h treatment ± 1 mM DFP in the presence or absence of 50 nM BafA1 for the final 2 h. Western blot from cell lysates shows representative ULK1 knockdown level. Graph represents the mean red only area per cell from fluorescence images normalised to control DMSO siNT cells ± SEM from n=4 independent experiments. Significance was determined by two-way ANOVA followed by Tukey's multiple comparison test. **c** U2OS IMLS cells treated with 1 mM DFP as in **a** and fixed for CLEM analysis. Inset of cell area in white box is shown by confocal analysis and EM section along with EM overlay. Scale bar = 5μm, inset = 1μm **d** Citrate synthase activity from U2OS cells treated for 24 h ± 1 mM DFP with final 16 h in the presence of 50 nM BafA1 or DMSO, values are normalised to DMSO control from n=6 (DMSO) or n=3 (+BafA1) independent experiments ± SEM. Significance was determined by two-way ANOVA followed by Sidak's multiple comparisons test. **e** U2OS whole cell protein abundance was determined by mass spectrometry following treatment ± 1 mM DFP 24 h. Mitochondrial proteins identified by GO analysis (Term = Mitochondrion) are highlighted in blue. f Mean T-test difference between Control and DFP samples for peptides identified in **e** matching GO terms related to cellular organelles. Bars represent Log_2 fold change (Control vs DFP) ± SEM, number on bars indicate how many protein targets are included in GO analysis. ** = $p < 0.01$, *** = $p < 0.001$, **** = $p < 0.0001$ and n.s = not significant in all relevant panels.

Figure 2

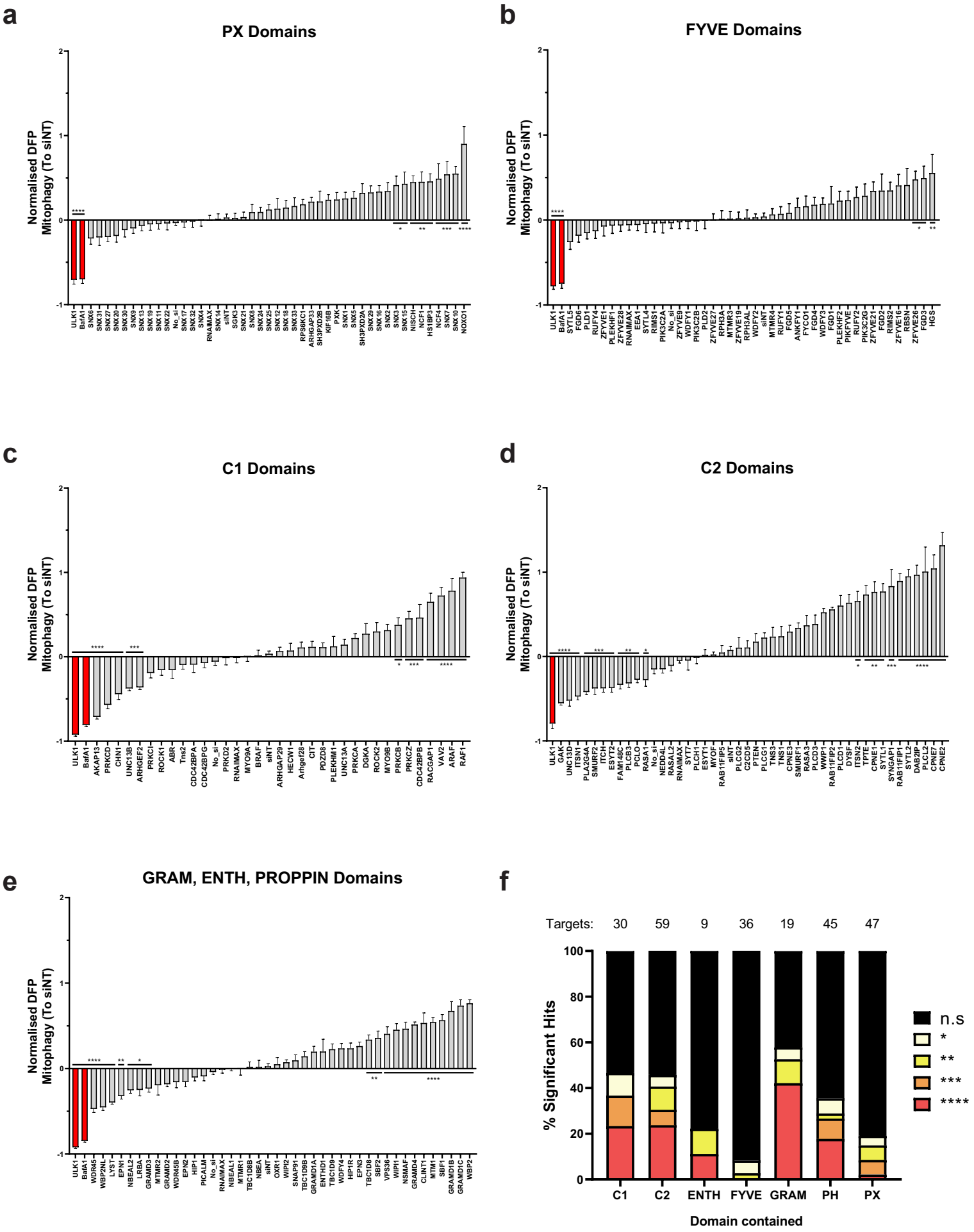

Figure 2 – siRNA screen for lipid binding proteins involved in DFP-induced mitophagy.

a-e Primary siRNA screen data. U2OS cells were transfected with a pool of 3 sequence variable siRNA oligonucleotides per gene target (2.5 nM per oligo) for 48 h before addition of 1 mM DFP for 24 h. Cells were PFA fixed and imaged using a 20x objective (35 fields of view per well). The red area per cell was normalised to the average of siNT controls and adjusted so that the DFP siNT control was 0 from n= 14 plates (**a**,**b**) or n=6 plates (**c-e**) ± SEM. siULK1 and BafA1 (red bars) are negative controls. siRNA targets containing similar lipid binding domains were assayed and plotted together as shown for **a** PX domains, **b** FYVE domains **c** C1 domains **d** C2 domains **e** GRAM, ENTH, PROPPIN domains. **f** Summary of significance of different lipid binding domains relative to the total tested from a e, proteins containing more than one type of domain are represented in each category. Significance was determined by one-way ANOVA followed by Dunnett's multiple comparison test to the siNT control where * = $p < 0.05$, ** = $p < 0.01$, *** = $p < 0.001$, **** = $p < 0.0001$ and n.s = not significant in all relevant panels.

Figure 3

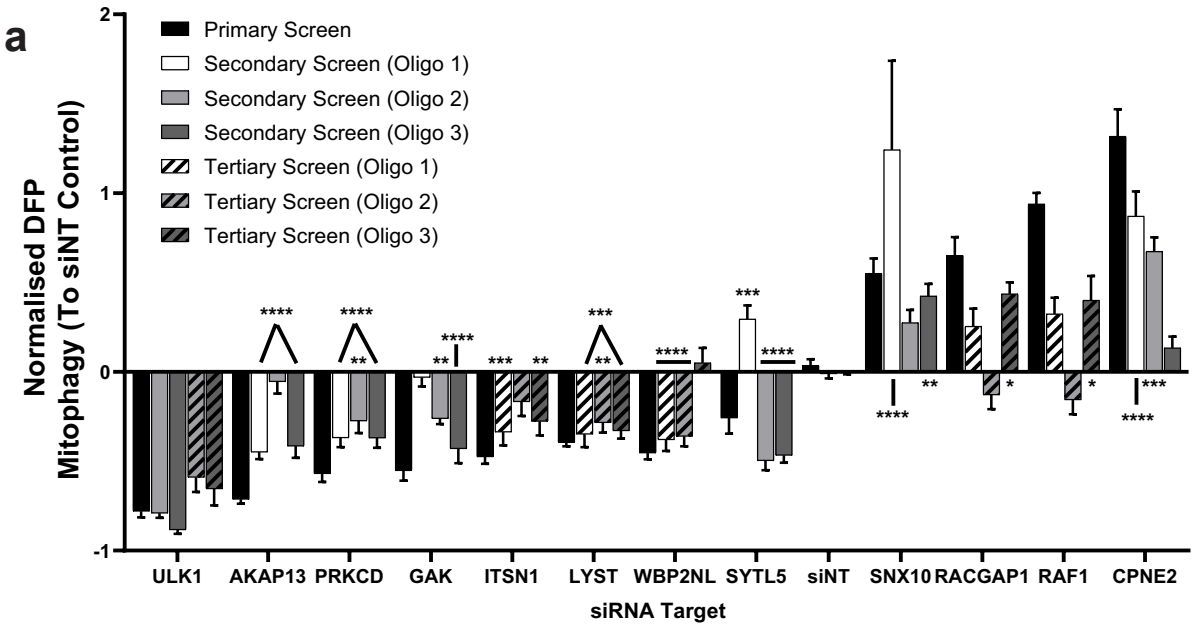

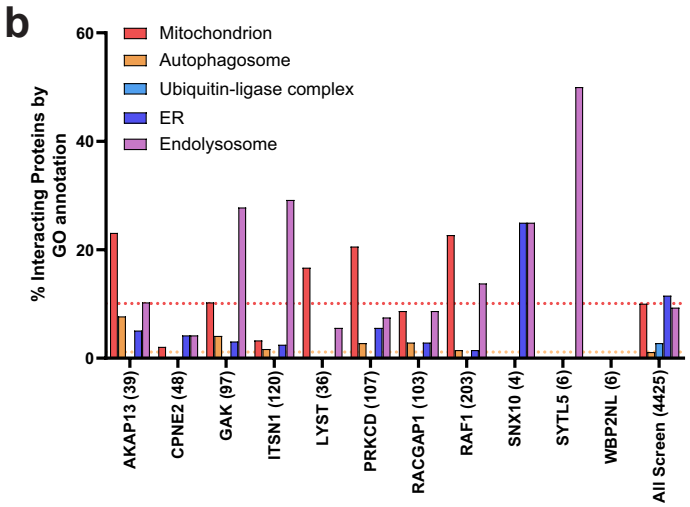

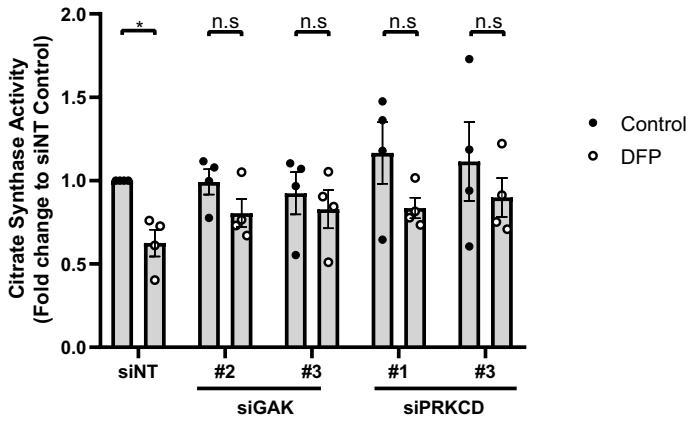

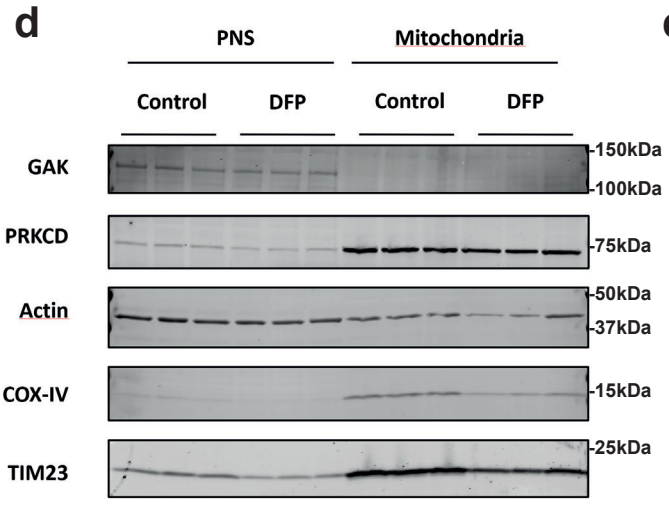

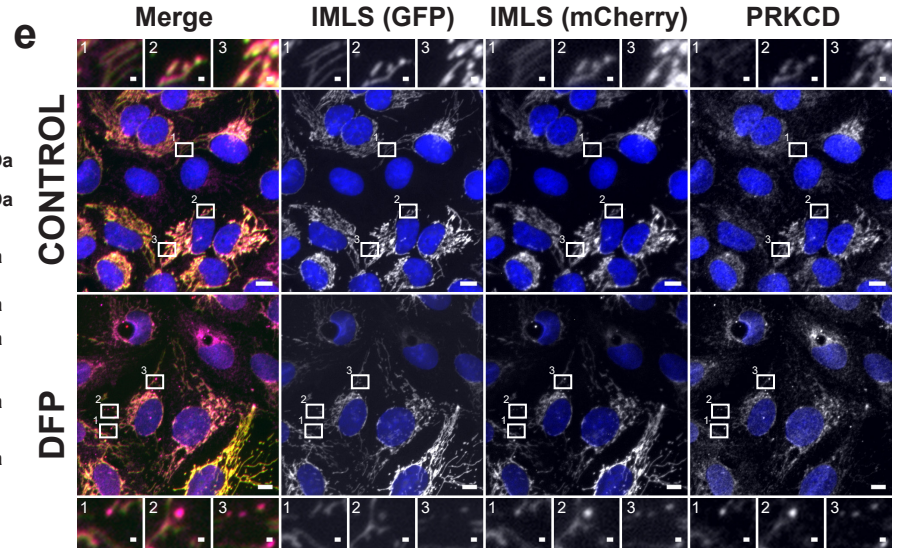

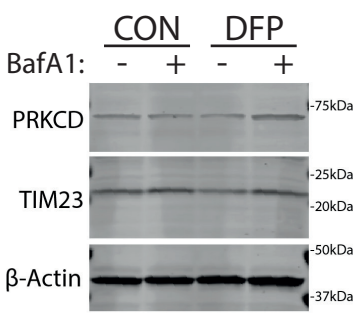

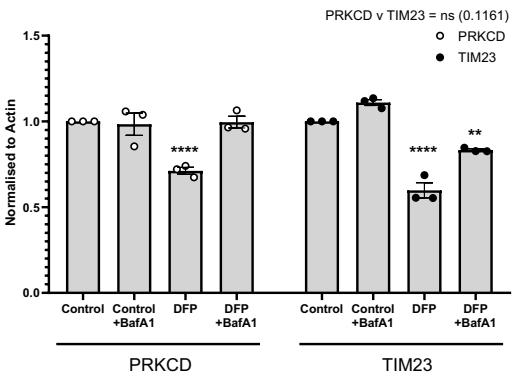

Figure 3 - GAK and PRKCD are regulators of DFP mediated mitophagy.

a Summary of significant targets identified across primary, secondary (7.5 nM individual siRNA oligos) and tertiary screen (15 nM each oligo) siRNA screens. Cells were transfected for 48 h prior to 24 h of 1 mM DFP treatment. Bars represent mean fold change in mitophagy relative to the siNT controls ± SEM. Significance was determined by one-way ANOVA followed by Dunnett's multiple comparison test to the siNT control. **b** Protein-protein interaction networks for candidate proteins (see methods) were plotted by % of interacting proteins belonging to each highlighted compartment, value in brackets represents total number of interacting proteins. **c** siRNA treatment with indicated oligos for 48 h prior to 24 h treatment ± 1 mM DFP and subsequent analysis of citrate synthase activity levels. Values were normalised to the siNT control and plotted ± SEM for n=4 independent experiments. Significance was determined by two-way ANOVA followed by Sidak's multiple comparison test. **d** U2OS cells treated ± 1 mM DFP for 24 h were enriched from a post-nuclear supernatant (PNS) for mitochondria followed by western blotting for the indicated proteins. **e** U2OS IMLS cells treated ± 1 mM DFP for 24 h followed by PFA fixation and staining for endogenous PRKCD (Alexa Fluor-647). Images were obtained by 20x objective using a Zeiss AxioObserver. Scale bar = 10 μm, insets = 1 μm. **f** U2OS cells treated ± 1 mM DFP for 24 h ± 50 nM BafA1 for the final 16 h and blotted for the indicated proteins. **g** Quantitation of PRKCD and TIM23 levels to β-actin in **f** from n=3 independent experiments ± SEM. Significance was determined by two-way ANOVA followed by Dunnett's multiple comparison test to the control. * = $p < 0.05$, ** = $p < 0.01$, *** = $p < 0.001$, **** = $p < 0.0001$ and n.s = not significant in all relevant panels.

Figure 4

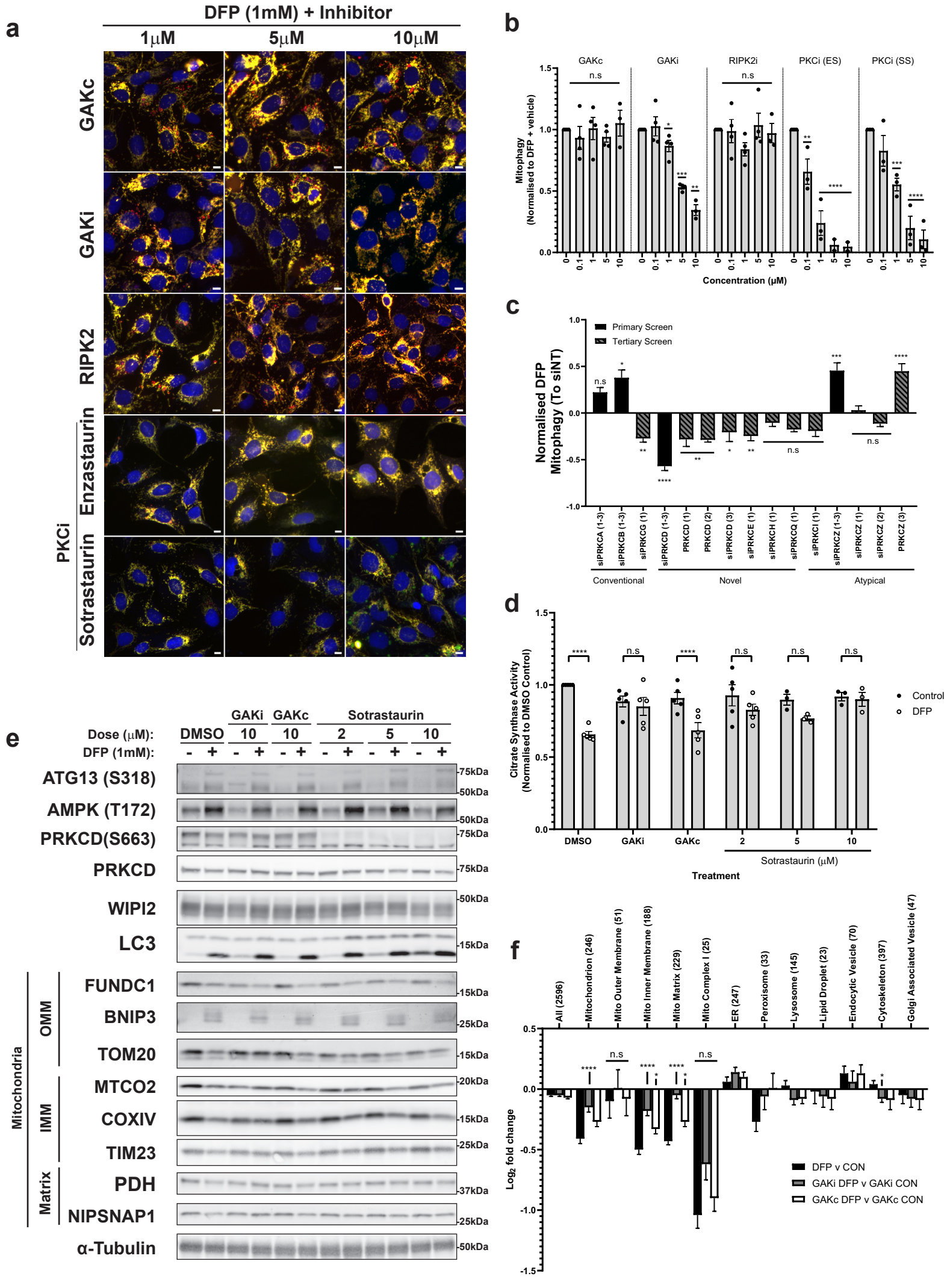

Figure 4 – GAK and PRKCD kinase activity regulates DFP-induced mitophagy

a Fluorescence images of U2OS IMLS cells treated with 1 mM DFP for 24 h in the presence of indicated inhibitors at stated concentrations (1-10 μM). Scale bar = 10 μm **b** Quantitation of cells red only structures normalised to DMSO + DFP control treatment. Significance was determined by two-way ANOVA followed by Dunnett's multiple comparison test to the DMSO + DFP control from a minimum of n=3 independent experiments. **c** U2OS IMLS cells treated with siRNA against indicated PKC isoforms (Primary screen = 7.5 nM, Tertiary = 15 nM) for 48 h prior to induction of mitophagy with 1 mM DFP for 24 h. Value in brackets represents oligonucleotide # used. Values represent mean fold change in mitophagy relative to the siNT control ± SEM from n=3 independent experiments. Significance was determined by one-way ANOVA to the relevant siNT control. **d** Citrate synthase activity of U2OS cells treated 24 h ± 1 mM DFP in combination with 10 μM GAKi, GAKc or 2-10 μM Sotrastaurin. Values represent mean citrate synthase activity normalised to DMSO control and plotted ± SEM from n=3 (Sotrastaurin 5/10μm) or n=5 independent experiments. Significance was determined by two-way ANOVA followed by Sidak's multiple comparison test. **e** U2OS cells were treated ± 1 mM DFP 24 h with GAKi or GAKc (10 μM), Sotrastaurin (2-10 μM) or DMSO control and western blotted for indicated proteins, including outer mitochondrial membrane (OMM), inner mitochondrial membrane (IMM) or Matrix proteins. **f** Cellular protein abundance was determined by mass spectrometry. U2OS cells were treated ± 1 mM DFP for 24 h in addition to DMSO, GAKi or GAKc (both 10 μM) and analysed by mass spectrometry. Comparison of mean abundance of GO annotated proteins between control and DFP treated samples for each GAKi, GAKc and DMSO control are shown ± SEM, value in brackets represent number of proteins classified in group by GO analysis. Significance was determined by two-way ANOVA followed by Dunnett's post-test to the DFP v CON sample. Significance is denoted in figure where: * = $p < 0.05$, ** = $p < 0.01$, *** = $p < 0.001$, **** = $p < 0.0001$ and n.s = not significant in all relevant panels.

Figure 5

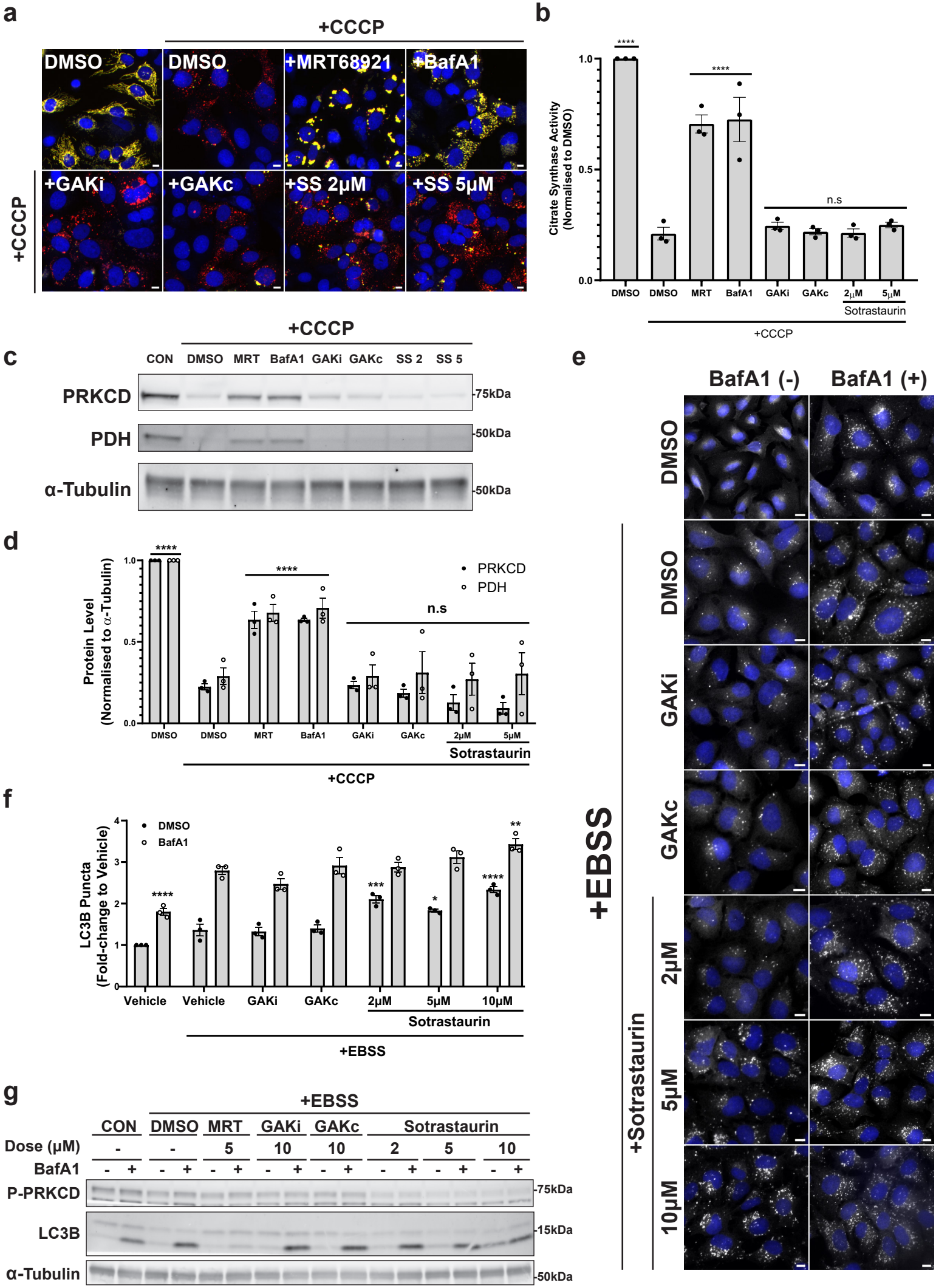

Figure 5 – GAK and PRKCD kinase activity are dispensable for PRKN-dependent mitophagy

a Representative fluorescence images of U2OS IMLS-PRKN cells treated for 16 h ± 20 μM CCCP and including 10 μM QVD-OPh to promote cell survival in addition to either MRT68921 (5 μM), BafA1 (50 nM), GAKi (10 μM), GAKc (10 μM) or Sotrastaurin (2-5 μM). Scale bar = 10μm **b** Cells treated as in **a** and assayed for citrate synthase activity and normalised to DMSO control. Mean value plotted ± SEM from n=3 independent experiments and significance determined by one-way ANOVA followed by Dunnett's multiple comparison to the CCCP+DMSO control. **c** Representative example of western blots from cells treated as in **a** and blotted for indicated proteins. **d** Quantitation of PRKCD and PDH levels from western blots in **c** from n=3 independent experiments ± SEM. Values represent protein level normalised first to α-Tubulin and subsequently normalised to the DMSO control. Significance was determined by two-way ANOVA followed by Dunnett's multiple comparison test to the DMSO control. **e** Representative 20x immunofluorescence images of U2OS cells stained for endogenous LC3B and nuclei (DAPI, blue). Cells were grown in complete media or EBSS (starvation) media for 2 h with addition of GAKi (10 μM), GAKc (10 μM) or Sotrastaurin (2-10μM) ± 50 nM BafA1, scale bar = 10 μm. **f** Quantitation of LC3B puncta from **e**. The average LC3 puncta per cell was normalised to that of the complete media control and represents the mean ± SEM from n=3 independent experiments . Significance was determined by two-way ANOVA followed by Dunnett's multiple comparison test to the EBSS vehicle treated sample. **g** Representative western blot of cells treated as in **e** and blotted for indicated proteins. * = $p < 0.05$, ** = $p < 0.01$, *** = $p < 0.001$ and **** = $p < 0.0001$ and n.s = not significant in all relevant panels.

Figure 8

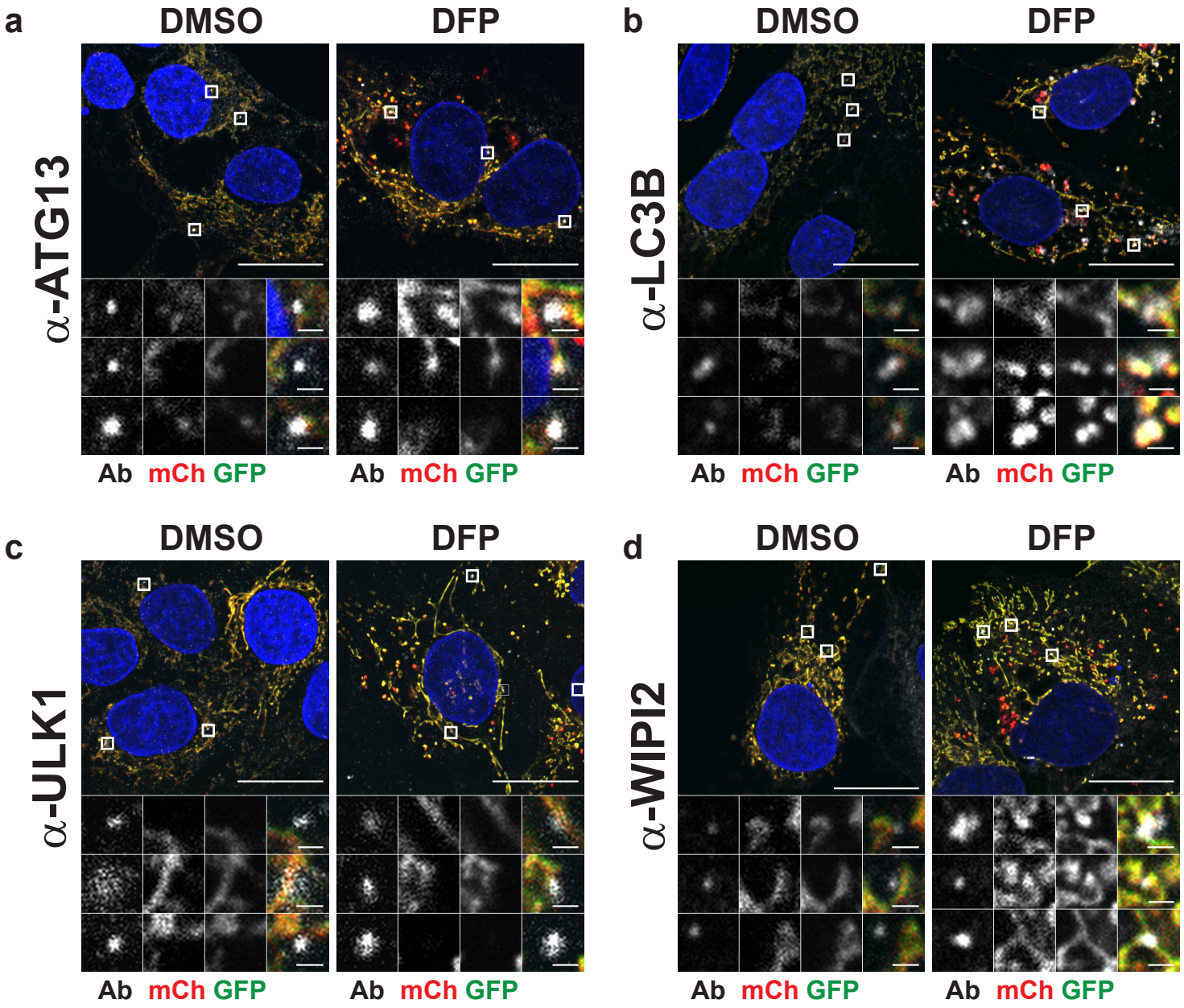

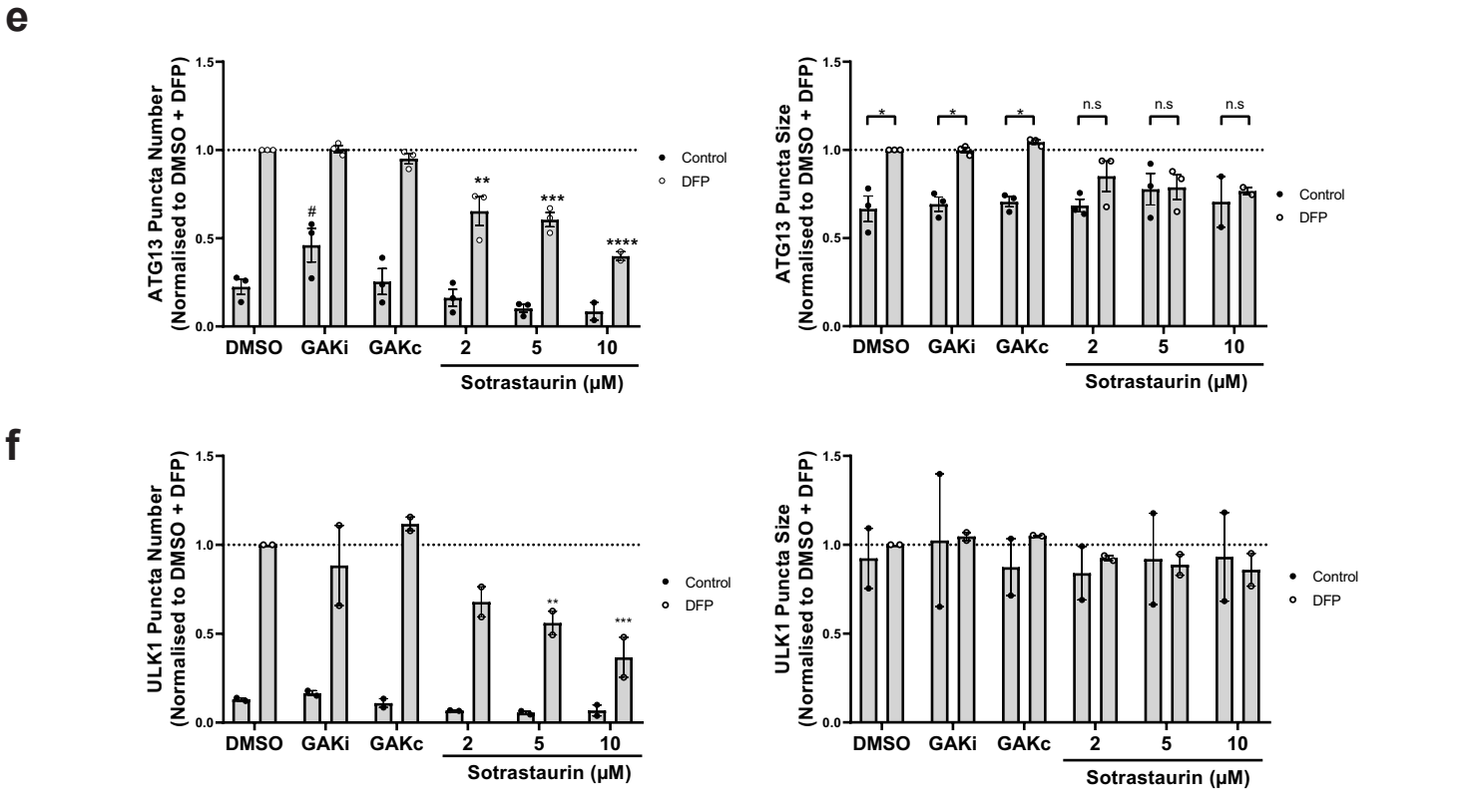

Figure 6 – Early autophagy protein recruitment is defective upon PKCi

a-d U2OS IMLS cells were treated ± 1 mM DFP for 24 h, fixed and stained for nuclei (DAPI) and the indicated endogenous autophagy markers; **a** ATG13, **b** LC3B, **c** ULK1 or **d** WIPI2. Representative 63x images of cells taken by Zeiss LSM 710 are shown, scale bar = 10 µm. **e-f** U2OS cells were treated ± 1 mM DFP for 24 h together with GAKi (10 µM), GAKc (10 µM) or Sotrastaurin (2-10 µM), then fixed in PFA before staining for nuclei (DAPI) and the indicated endogenous early autophagy markers; **e** ATG13, **f** ULK1. The number and size of puncta formed for each marker was analysed and values obtained were normalised to the DMSO + DFP control. Mean values were plotted from n=3 independent experiments ± SEM. Significance was determined by two-way ANOVA and Dunnett's multiple comparisons test to the DMSO+DFP control sample where * = $p < 0.05$, ** = $p < 0.01$, *** = $p < 0.001$, **** = $p < 0.0001$, n.s = not significant and # = $p < 0.05$ (to the DMSO Control).

Figure 7

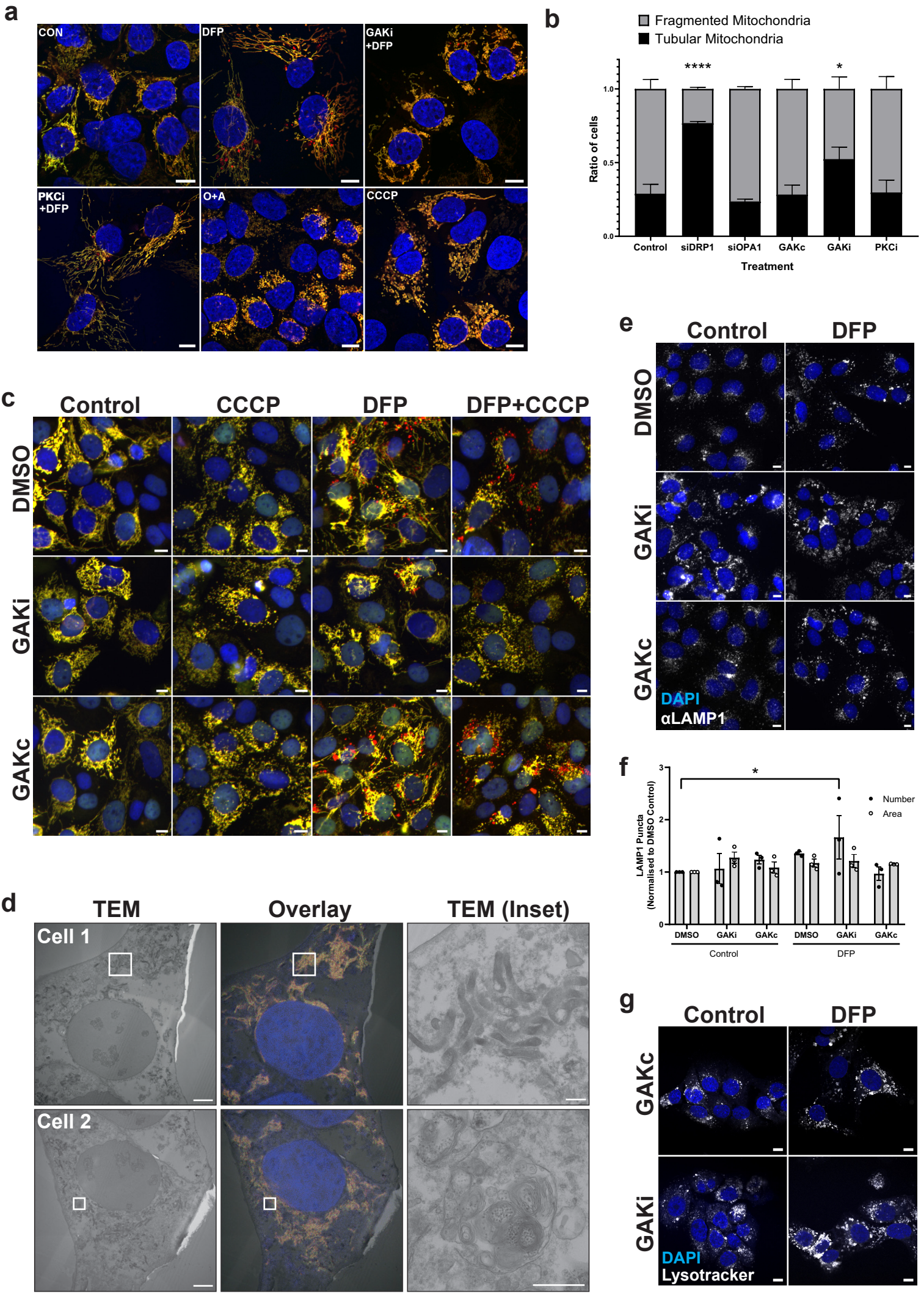

Figure 7 – GAKi induces abnormal mitochondrial and lysosomal morphology

a Representative 63x images of U2OS IMLS cells taken by Zeiss LSM 710 confocal microscopy. Cells were treated ± 1 mM DFP 24 h in addition to GAKi (10 μM), Sotrastaurin (PKCi – 2 μM), Oligomycin and Antimycin A (O+A – 10 μM and 1 μM respectively) or CCCP (20 μM), scale bar = 10 μm. **b** Machine learning classification of U2OS IMLS cell mitochondrial network as fragmented or tubular (utilising EGFP images, see methods) after 24 h treatment with GAKi (10 μM), GAKc (10 μM) or Sotrastaurin (PKCi – 2μM) compared to 72 h knockdown of non-targeting control, siDRP1 or siOPA1. Significance was determined by two-way ANOVA followed by Dunnett's post-test to the control treatment. **c** U2OS IMLS cells were treated as indicated with DMSO, GAKi or GAKc (10 μM each) for 24 h in addition to either DFP (24h, 1 mM), CCCP (20 μM, 12 h) or in combination. Images obtained by 20x objective, scale bar = 10μm. **d** U2OS IMLS cells were treated with 1 mM DFP + 10 μM GAKi for 24h prior to fixation for CLEM analysis. EM images demonstrate mitochondrial clustering (Cell 1) and an increase in autolysosome structures (Cell 2) induced by GAKi treatment, scale bar = 10 μm, inset = 1 μM. **e** U2OS cells treated ± 1 mM DFP 24 h in addition to DMSO, GAKi (10μM) or GAKc (10μM) were PFA fixed and subsequently stained for endogenous LAMP1. Images acquired by widefield microscopy on a Zeiss AxioObserver microscope, scale bar=10 μm. **f** Quantitation of LAMP1 structures identified in **e** for size and number from n=3 independent experiments and plotted as mean ± SEM. Significance was determined by two-way ANOVA followed by Dunnett's multiple comparisons test to the DMSO control. **g** U2OS cells were treated for 24 h ± 1 mM DFP with either GAKc (10 μM) or GAKi (10 μM) and then stained for lysosomes using lysotracker red DND-99 at 50 nM. Representative images taken by Zeiss LSM710, scale bar = 10 μm. Significance was denoted where * = $p < 0.05$, **** = $p < 0.0001$ and n.s = not significant.

Figure 8

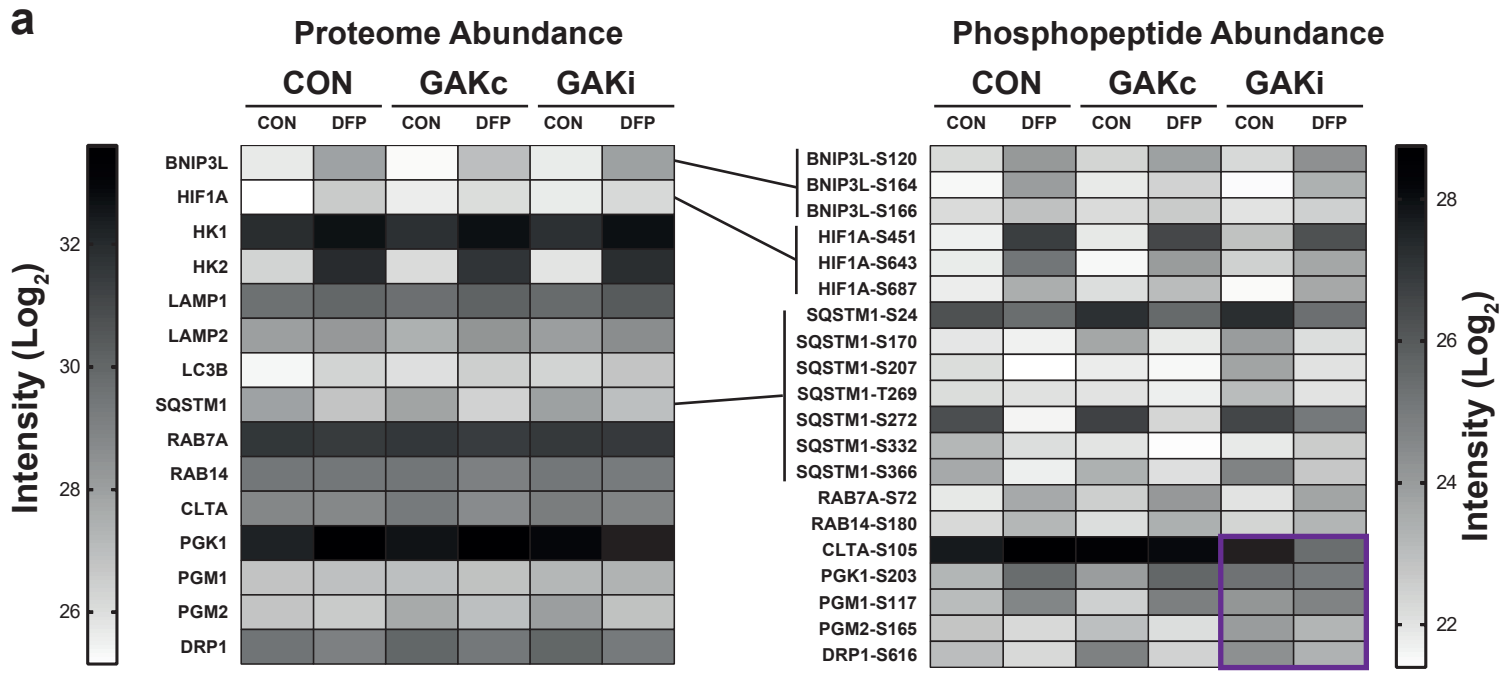

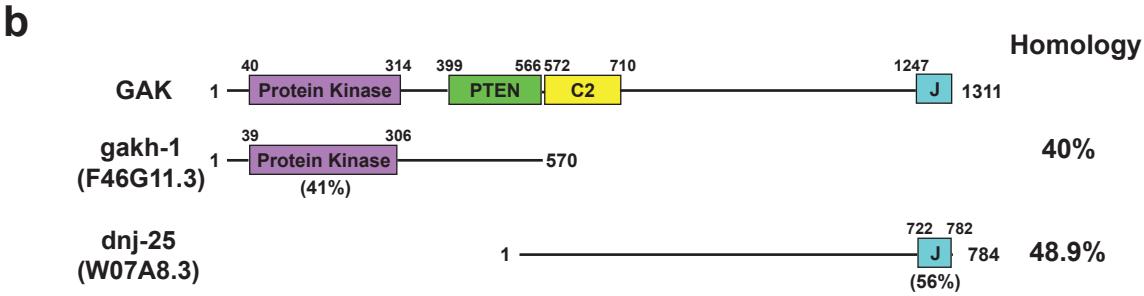

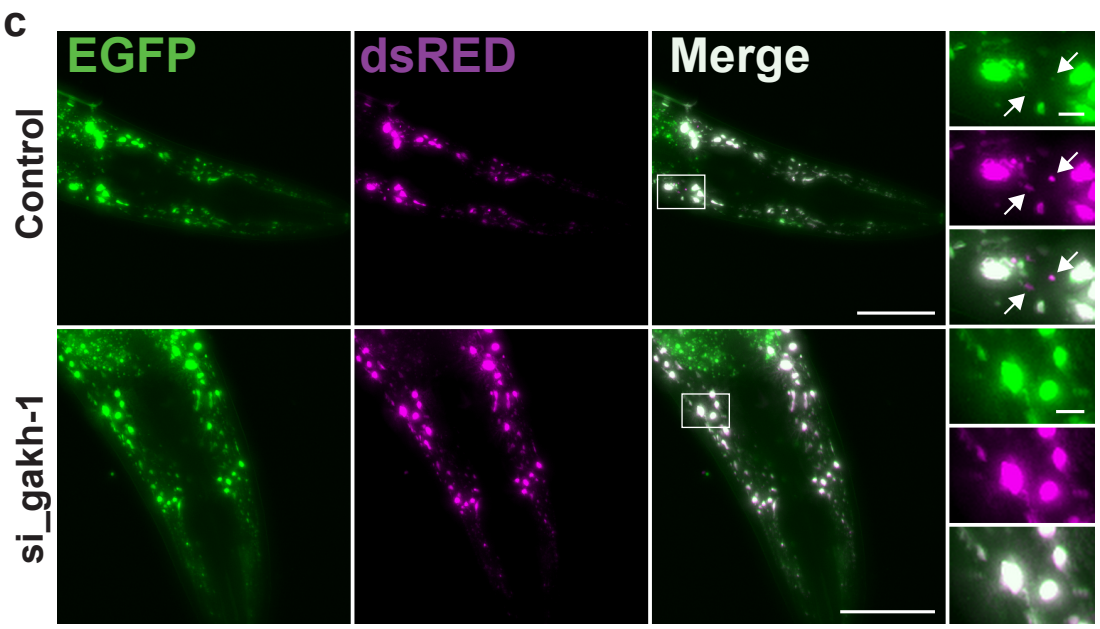

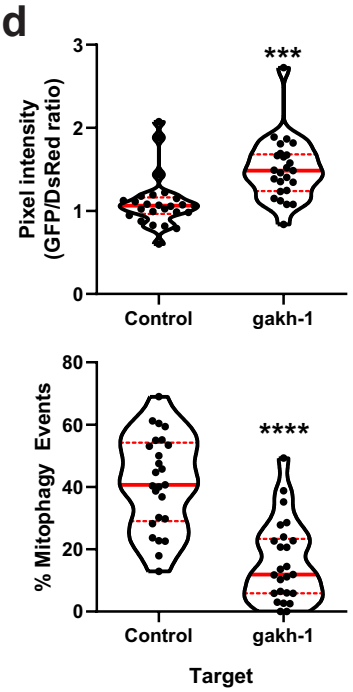

Figure 8 – gakh-1 regulates mitophagy in vivo

a Mass spectrometry of DFP and GAKi regulated proteins/phospho-peptides. U2OS cells were treated ± 1 mM DFP for 24 h in combination with DMSO vehicle, GAKi or GAKc (both 10 μM). Cell pellets were collected and split between proteome and phospho-peptide analysis (see methods). Data represents average intensity from n=2 independent experiments. **b** Schematic representation of GAK domain structure and orthologues gakh-1 and dnj-25 present in C.elegans. Homology values were obtained by protein blast alignment. **c** In vivo detection of mitophagy in C. elegans. Transgenic nematodes expressing mtRosella in bodywall muscle cells were treated with gakh-1 RNAi or pL4440 control vector. dsRED only structures represent mitochondria in acidic compartments (arrowheads). Scale bar = 50 μm, inset = 5 μm. **d** Mitophagy stimulation signified by the ratio between pH-sensitive GFP to pH insensitive dsREd (n= 25, upper panel). Quantification of the frequency of mitochondria undergoing mitophagy (dsREd puncta lacking EGFP co-localisation) are expressed as percentage of total mitochondria detected (n= 25, lower panel). The data is presented as violin plots of individual values with median (red, solid line) and quartiles (red, dashed line) shown. Significance was determined by unpaired two tailed t-test from n=2 independent experiments, where *** = $p < 0.001$ or **** = $p < 0.0001$.

Figure 9

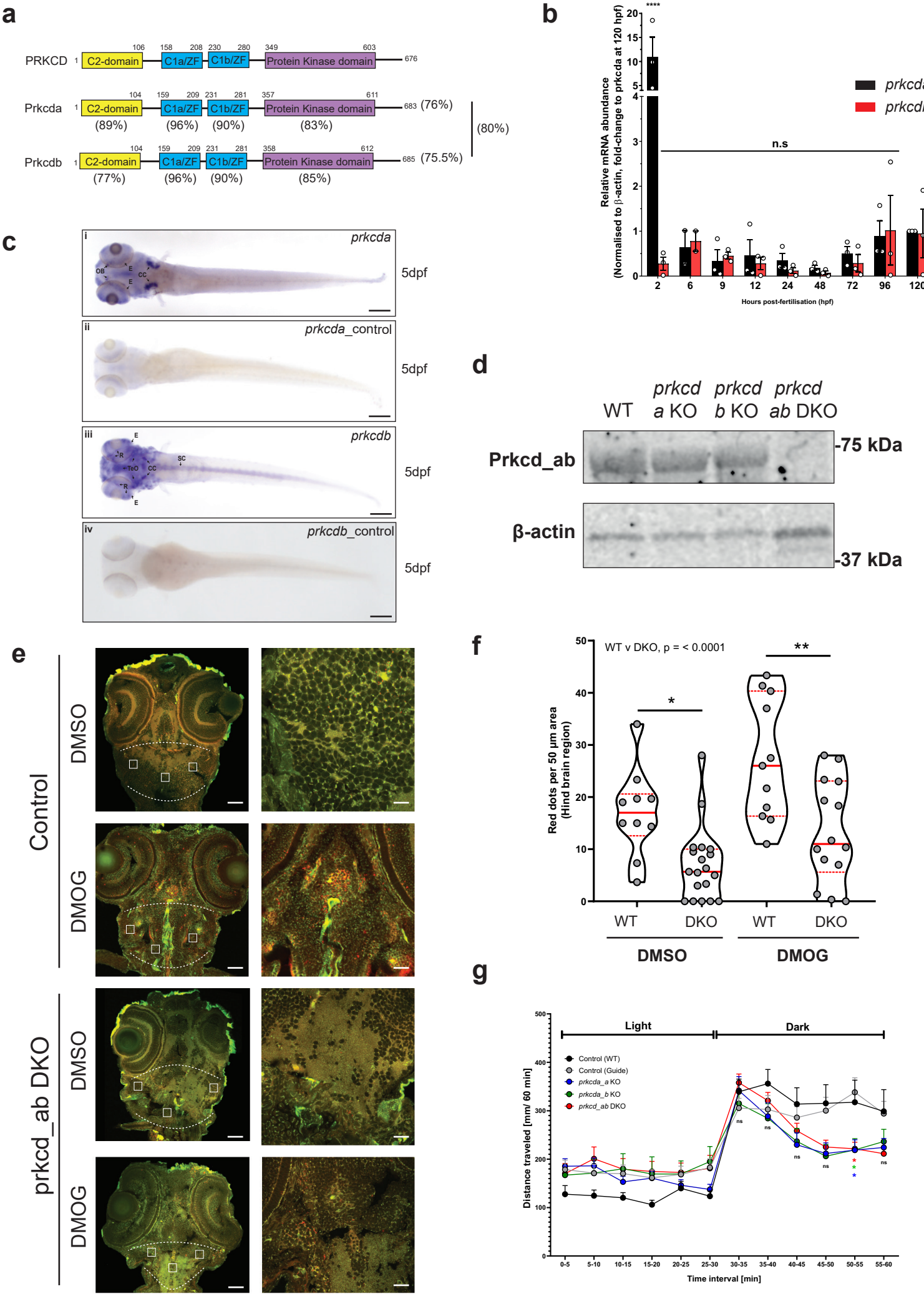

Figure 9 – prkcda and prkcdb regulate mitophagy in vivo

a Overview and schematic diagram of human PRKCD, zebrafish prkcda and prkcdb proteins. Percentage identity of respective domains on comparison with human counterpart shown below the zebrafish domains. Also shown is the percentage identity of the protein amongst each other. **b** Temporal expression pattern of prkcda and prkcdb. The graph shows the mean relative transcript abundance in whole zebrafish embryos from 2 hpf to 5 dpf from n=2 (6 hpf) or n=3 (all others) independent experiments **c** Spatial expression pattern of prkcda and prkcdb at 5 dpf as demonstrated by whole mount in situ hybridisation at the indicated stage using a 5'UTR probe. Both the larvae are in dorsal view. Scale bar = 200 μ m. **d** Representative immunoblots of Prkcd and β-actin on whole embryo lysates from wild-type and single or double prkcda/prkcdb KO (DKO) animals. **e** Representative confocal images of cryosections taken from control (guide only) and prkcd_ab DKO transgenic tandem-tagged mitofish larvae treated with DMSO only or with DMOG at 3 dpf. Images are from the hind brain region of the respective larvae as marked. Scale bars = 50 μm (left), 20 μm (right). **f** The graph shows the average number of red puncta from three 50 μm hind brain region (as marked in e) from each of 10-19 larvae for control and prkcd_ab DKO tandem-tagged mitofish larvae. Significance was determined by two-way ANOVA followed by Tukey's post-test to compare all groups. **g** Motility analysis of zebrafish embryos at 5 dpf using the "Zebrabox" automated videotracker (Viewpoint). Assay was carried out during daytime, and consisted of one cycle of 30 min exposure to light followed by 30 min of darkness. Data represents mean distance moved ± SEM. Each group consisted of 43-124 larvae from n= 9 independent experiments. Significance was determined by two-way ANOVA followed by Dunnett's post-test to the Control (WT). Significance are denoted where *$p < 0.05$, **$p < 0.01$, ***$p < 0.001$, **** $p < 0.0001$, n.s = not significant.